Simplified Vehicle Control Concept for a Lift Plus Cruise eVTOL Vehicle

John Kaneshige* Thomas Lombaerts† Kimberlee Shish‡ Michael Feary§
NASA Ames Research Center, Moffett Field, CA 94035

Electric Vertical Takeoff and Landing (eVTOL) vehicles have the potential to enable cost effective Urban Air Mobility (UAM) applications. These concepts may also pose several challenging handling and control problems, which must be addressed prior to safe and reliable urban operations. This paper investigates a simplified vehicle control concept that is designed to address some of these challenges for a conceptual Lift Plus Cruise vehicle designed by NASA's Revolutionary Vertical Lift Technology (RVLT) project. The command and control architecture for this concept is presented along with preliminary findings. Initial results explore the vehicle performance in an approach to hover transition scenario, designed to explore the challenge of dissipating energy across all flight regimes. Operational concepts with varying aggressiveness are evaluated through changing glideslope and deceleration rates. Preliminary results show that the simplified control concept is effective over these operational conditions, with control strategies and envelope protection limits able to maintain control though aggressive operations despite saturation at steeper slopes with higher deceleration rates. Final results will show piloted simulation evaluations in the the Aerospace Cognitive Engineering Lab – Rapid Automation Test Environment (ACEL-RATE) laboratory at NASA Ames Research Center. The planned tests will build on these operations with additional test cases exploring variations in wind conditions as well as transition-to-hover automation strategies and display information.

Nomenclature

α	angle of attack [rad]
β	sideslip angle [rad]
$\mathbf{\Omega}$	rotation matrix
χ	track angle [rad]
Δ	difference / change
δ	deflection [rad]
γ	flight path angle [rad]
ϕ	bank angle [rad]
ψ	yaw angle [rad]
τ	time constant [s]
$\dot{h}$	climb/sink rate [ft/s]
$\dot{z}$	earth referenced vertical speed [ft/s]
$\overline{q}$	dynamic pressure, $= \frac{1}{2}\rho V_{\text{TAS}}^2$ [lbs/(ft s^2)]
C	coefficient [-]
D	drag [lbs ft/s^2]
dt	time step [s]
E	distance East [ft]
g	gravitational acceleration [ft/s^2]
h	altitude [ft]
K	controller gain [-]
L	lift [lbs ft/s^2]
m	mass [lbs]
N	distance North [ft]
n	load factor [-]
r	yaw rate [rad/s]
R_e	Earth radius [ft]
S	wing surface area [ft^2]
T	Thrust [lbs ft/s^2]
u	forward velocity component [ft/s]
V	speed [kts]
v	lateral velocity component [ft/s]
W	weight [lbs ft/s^2]
w	vertical speed component [ft/s]
X	distance along the nose X-axis [ft]
Y	distance along the wing Y-axis [ft]
Y	lateral axis or lateral force [lbs ft/s^2]
Z	vertical axis
lat	latitude [deg]
lon	longitude [deg]
B or b	body referenced
GS	ground speed
0	at sea level
aero	aerodynamic
CAS	calibrated airspeed
cmd	commanded
comp	computed
ctl	control

*Computer Engineer, Intelligent Systems Division, Mail Stop 269-1, AIAA member, email: john.t.kaneshige@nasa.gov.
†Aerospace Research Engineer, KBR, Intelligent Systems Division, Mail Stop 269-1, AIAA Associate Fellow, email: thomas.lombaerts@nasa.gov.
‡Aerospace Engineer, Intelligent Systems Division, Mail Stop 269-1, AIAA member, email: kimberlee.h.shish@nasa.gov.
§Aerospace Technologist, Human Systems Integration Division, Mail Stop 262-1, AIAA member, email: michael.s.feary@nasa.gov.

env	envelope protected	pos	position
hov	hover	TAS	true airspeed
lim	limited	TC	turn coordination
perf	performance	thr	throttle

I. Introduction

WINGED electric Vertical Takeoff and Landing (eVTOL) vehicles that can takeoff and land vertically like a helicopter and cruise like an airplane have the potential of increasing operational capabilities while maintaining a high degree of efficiency. Some designs have separate vertical and forward propulsion systems (e.g., a lift plus cruise vehicle), others have a tilting propulsion system (e.g., a tilt-rotor or tilt-wing vehicle), and hybrid designs have a combination of both concepts (e.g., with both vertical and tilting propulsion systems) [1]. During low speed and hover maneuvering, the vertical propulsion system provides the primary source of lift and maneuvering. As these vehicles transition between hover and forward flight, the vertical and/or tilting propulsion systems can be used to compensate for the changing amount of lift produced by the wings (e.g., to prevent the vehicles from stalling). Once sufficient airspeed is obtained, these vehicles can be controlled by manipulating traditional flight control surfaces. Upon reaching forward flight, the wings can produce all of the necessary lift, so the vertical propulsion systems can stop and/or the tilting propulsion systems can rotate forward.

Like all eVTOL vehicles, winged eVTOL vehicles suffer from slow response times during low speed and hover maneuvering. This is due to the multiple lifting rotor configuration that enables maneuvering by manipulating the thrust produced by individual rotors. Unlike a helicopter, the individual rotor blades are not cyclically controlled (i.e., so that it will have the same angle of incidence as it passes the same point in the cycle). Some rotors use a fixed blade pitch design, and manipulate thrust by modifying rotor speed (similar to smaller quadcopter drones). Other rotors use a variable blade pitch design, and manipulate thrust by collectively modifying the pitch angle of all the blades on an individual rotor (similar to the collective control of a helicopter). The latter has the advantage of faster rotor response times, but at a higher weight penalty [2]. However, both designs will typically have significantly slower maneuvering response times compared to a helicopter.

Compared to multicopters, winged eVTOL vehicles are more susceptible to wind changes (e.g., due to gusts or changes in the vehicle's orientation with respect to the wind). As these vehicles transition between hover and forward flight, they will also encounter significant aerodynamic changes (e.g., the amount of lift produced by the wings and the amount of stabilizing pitch and yaw moments produced by the horizontal and vertical tails). As a result, these vehicles will respond differently as they transition between hover and forward flight. While these vehicles may be stable in forward flight, they are by design inherently unstable in hover and warrant the use of indirect flight control systems to provide stability and control augmentation. Furthermore, the slow response (at low speeds and hover) coupled with the changing nature of flight (when transitioning between hover and forward flight) may also necessitate higher-level outer loop control systems with a simpler pilot interface.

Simplified Vehicle Operations (SVO) is a term adopted by the aviation community for "the use of automation to reduce the number of skills a pilot or operator of an aircraft must acquire to achieve the required level of operational safety." [3] The term Simplified Vehicle Controls (SVC) is meant to convey a subset that focuses on the aircraft handling skill category. The SVC concept described in this paper was inspired by previously developed ideas. The 'Unified' control concept was initially developed specifically for VTOL vehicles by the UK's RAE (Royal Aircraft Establishment) in the 1970's and 80's [4]. It was first tested on the Vectored thrust Aircraft Advanced Control (VAAC) for the AV-8B Harrier [5], and this concept was recently further developed and implemented in the F-35B Lightning II [6, 7]. Another concept is based on the so-called 'E-Z Fly' control concept, developed at NASA Langley in the 1990's [8]. This concept decoupled the flight controls of a general aviation aircraft. This decoupling made the airplane "easy to fly", even for novice pilots. Both concepts have been developed further and adapted specifically for application in winged eVTOL vehicles in the context of UAM operations [9–11].

This paper examines an SVC concept, along with corresponding pilot interfaces (i.e., inceptor implementations and display elements), to evaluate the effectiveness in compensating for control-related challenges of a conceptual Lift Plus Cruise (LPC) vehicle. The outline of this paper is as follows. First, the LPC vehicle model and inner loop stability and control augmentation system are described in Sec. II. Next, the SVC concept is discussed in Sec. III. Thereafter, Sec. **??** describes the simulation evaluations conducted, together with some specific results. Finally, the paper wraps up with a summary and conclusions in Sec. V.

II. Lift Plus Cruise Vehicle

The Lift Plus Cruise (LPC) conceptual model was designed by NASA's Revolutionary Vertical Lift Technology (RVLT) project [12]. The vehicle is designed to takeoff vertically like a helicopter, transition to fly in forward flight like an airplane, and then transition back to land vertically like a helicopter. The vehicle can optimize power consumption efficiency by staying on the wing as long as possible. As a result, the proposed operational concept is to quickly accelerate just after takeoff, and to quickly decelerate to hover just prior to landing. A description of the vehicle model is provided in Sec. II.A, and an overview of the inner loop control system over flight regimes is provided in Sec. II.B.

A. Vehicle Model

The vehicle has a design gross weight of 6,000 lbs (with a payload of 1,000 lbs), range of 50 nautical miles, and maximum speed of 120 knots. It has eight lifting rotors and one pusher propeller, as shown in Fig. 1. The vehicle also has flight control surfaces consisting of two ailerons, an elevator and a rudder. The lifting rotors and the pusher propeller are of a variable blade pitch angle design, and operate at a constant number of Rotations Per Minute (RPM). The amount of thrust produced by each rotor and the propeller can be independently manipulated by collectively adjusting the pitch angle of the blades. Collectively manipulating all rotors (1-8) will adjust the force along the heave axis. Manipulating the forward rotors (1-4) in the opposite direction as the rear rotors (5-8) will generate a pitch moment. Manipulating the left rotors (1-2, 5-6) in the opposite direction as the right rotors (3-4, 7-8) will generate a roll moment. Manipulating the counterclockwise spinning rotors (1, 3, 6, 8) in the opposite direction as the clockwise spinning rotors (2, 4, 5, 7) will generate a yaw moment. In forward flight, the lifting rotors are stopped at a neutral position and the vehicle is controlled using flight control surfaces, with the pusher propeller providing forward propulsion. Without the lifting rotors, the stall speed of the vehicle is approximately 80 knots.

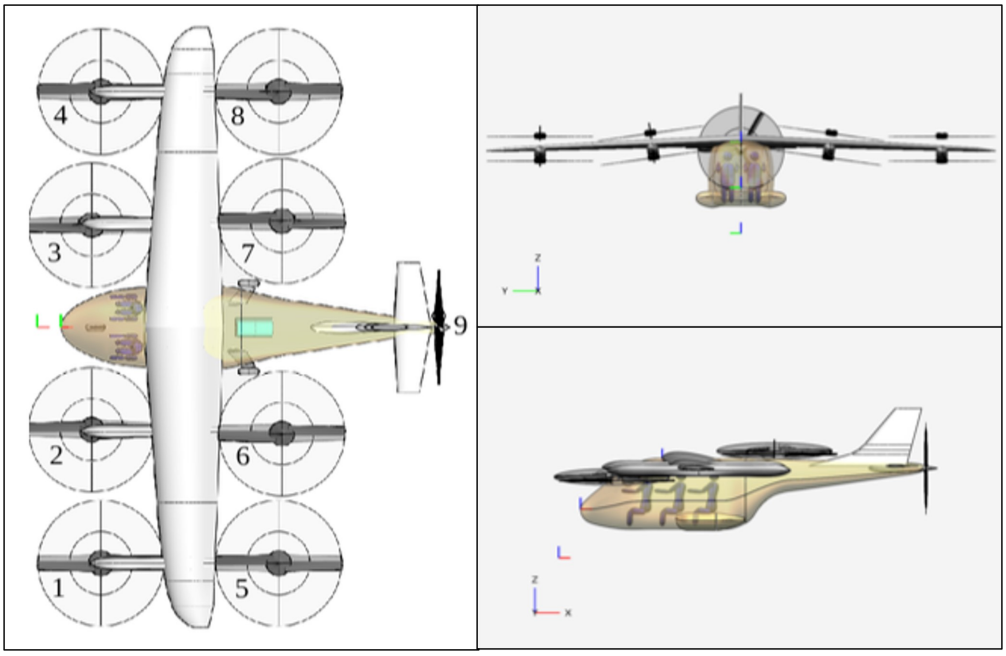

Fig. 1 Lift Plus Cruise (LPC) concept vehicle

The dynamic model was generated by Advanced Rotorcraft Technology (ART) using FlightLAB [13, 14]. This model was integrated into a flight simulation environment that was designed to enable rapid integration and evaluation of new vehicle models. The original quasi-Linear Parameter Varying (qLPV, a common rotorcraft representation [15, 16]) model was modified to apply nonlinear kinematic and gravitational terms (in place of linearized terms). The model inputs consist of the collective pitch angle for each lifting rotor and the pusher propeller, and deflection angles for the ailerons, elevator and rudder. The final simulation model also includes (1st and 2nd order) actuator models, a gear/ground model, a NASA Dryden-based turbulence model and a FAA-based wind gust model [17]).

B. Inner Loop Control System

The architecture of the inner loop control system was designed to enable rapid integration and evaluation of new vehicle models. A Nonlinear Dynamic Inversion (NDI) based flight control system is used to provide inner loop stability and control augmentation [18, 19]. The integration process begins by determining the control allocation and mixing strategies for all of the control effectors. Then the desired inner loop control modes (corresponding to ADS-33 response types [20]) are determined. Analysis of the open-loop dynamics of the vehicle is used to specify the reference model and error controller gains that correspond to the control system for each control mode. These mode specific controllers generate acceleration commands that are used to compute control effector commands through model inversion. An overview of the controller architecture can be seen in Fig. 2, along with descriptions of the control allocation and control mode schedule in Sec. II.B.1 and II.B.2, respectively.

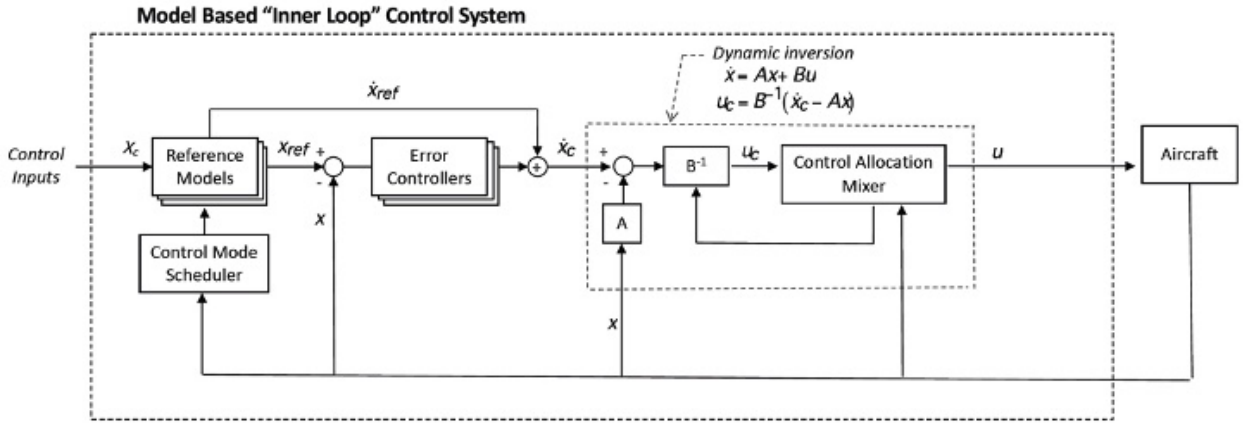

Fig. 2 Inner Loop Control System

1. Control Allocation

The control allocation for the lifting rotors, pusher propeller, and flight control surfaces are specified according to the operating flight regimes specified in Fig. 3. The flight regime schedule is a function of airspeed, with varying accelerating and decelerating transition speeds to avoid hysteresis. For example the transitions from hover-to-transitional and transitional-to-forward flight regimes occur at 40 and 100 knots respectively. Conversely, the transitions from forward flight-to-transitional and transitional-to-hover flight regimes occur at 90 and 30 knots respectively.

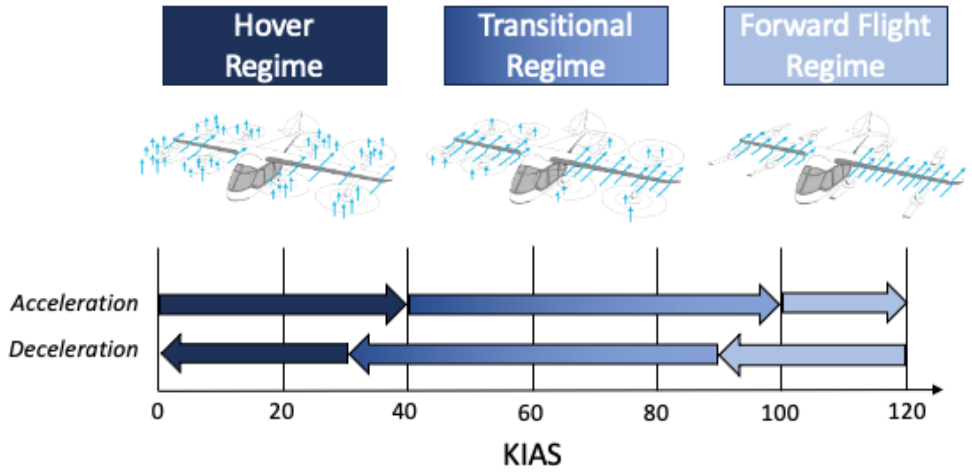

Fig. 3 Flight Regime Schedule

The control allocation schedule is illustrated in Fig. 4. In the hover regime, the lifting rotors are used collectively to produce lift for controlling the heave-axis, and differentially for maneuvering to control the pitch, roll and yaw axes. In the transitional regime, the lifting rotors are used differentially in combination with the flight control surfaces for maneuvering. Meanwhile, the lifting rotors are still used collectively to provide some lift (e.g., for angle-of-attack protection). In the forward flight regime, the lifting rotors are stopped at a neutral position and the vehicle is controlled using flight control surfaces, with the pusher propeller providing forward propulsion.

Control Effectors	Hover Regime	Transitional Regime	Forward Flight Regime
Collective Rotors	Heave Axis		- - -
Differential Rotors	Pitch/Roll/Yaw Axes		- - -
Flight Control Surfaces	- - -	Pitch/Roll/Yaw Axes	
Rear Propeller	Thrust Axis		

Fig. 4 Control Allocation Schedule

For the lifting rotors, each axis (i.e., roll, pitch, yaw and heave) was assigned an allocation of 33 percent around a trim point of 50 percent. As a result, a single axis of control had a range of 17 to 83 percent of full authority. This allocation is needed to determine the B-matrix in the dynamic inversion calculations. While the allocation scheme does not prevent against actuator saturation, consideration was given to saturation in the dynamic inversion calculations. To allow some compensation for saturation, the dynamic inversion calculation is iteratively recomputed with inputs fixed at maximum values if they exceed their allocation.

2. Inner Loop Control Modes

Inner loop control modes were determined with consideration to vehicle operation and performance. As a result, control modes are scheduled automatically as a function of flight regime. The schedule of the control modes used in this evaluation are displayed in Fig. 5. While most of these control modes have heritage in ADS-33 [20], some new ones were added for enabling simplified operations. Each of these modes consists of a reference model and error controller.

Control Axes	Hover Regime	Transitional Regime	Forward Flight Regime
Heave Axis	Rate Command Height Hold (RCHH)	Angle-of-Attack Command (AOAC)	- - -
Pitch and Roll Axes	Rate Command Attitude Hold (RCAH)		
Yaw Axis	Rate Command Direction Hold (RCDH)	Turn Coordination (TC)	
Thrust Axis	Acceleration Command Speed Hold (ACSH)		

Fig. 5 Control Mode Schedule

Pitch, roll and yaw control modes provide rotational stability and control augmentation. The rotational control modes consisted of Rate Command Attitude Hold (RCAH) for pitch and roll control, and Rate Command Direction Hold (RCDH) and Turn Coordination (TC) for yaw control. For the yaw modes, RCDH provides yaw control at lower speeds (i.e., in the hover regime). Once aerodynamic effects take effect (i.e., in the transitional and forward flight regimes), sideslip considerations necessitate the use of TC. Translational modes include Rate Command Height Hold (RCHH) and Angle-of-Attack Command (AOAC) for heave, and Acceleration Command Speed Hold (ACSH) for thrust. When

at lower speeds, the collective lifting rotors can provide direct altitude control through RCHH. As aerodynamic effects influence vehicle behavior, AOAC supports an angle-of-attack protection system. ACSH allows for simplified speed control (i.e., the magnitude of the velocity vector).

The inner loop control system corresponding to each mode generally consists of a reference model and an error controller (Fig. 6). This setup allows for decoupling of the gain tuning according to the purpose. The gains in the reference model serve for command shaping, i.e. the responsiveness of the vehicle to a commanded input. The PID gains of the error controller tune how quick disturbances (such as turbulence induced deviations) are compensated for. More technical details on the different aforementioned inner loop control systems are given in Appendix VI.A.

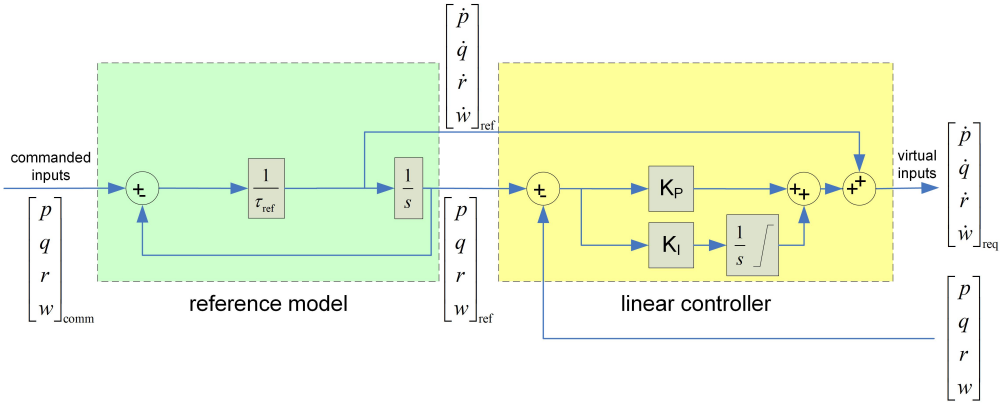

Fig. 6 Block diagram of command filtering, reference model and linear controller

III. Simplified Vehicle Control Concept

One of the many challenges that eVTOL vehicles face is a complex flight control task over different flight regimes. While the inner loop control system can provide stability and control augmentation for the rotational (pitch, roll, yaw) and translational (heave and thrust) axes, conventional command and control of these axes will have a different effect on the vehicle's speed and flight path as it transitions between hover to forward flight. For example, pitching the nose of the aircraft up will primarily cause the vehicle to decelerate in the hover regime and climb in the forward flight regime. As a result, pilots would need to alter their control strategies when transitioning between flight regimes to maintain a constant flight path vector.

The SVC concept incorporates vector-based commands (i.e., where inceptor inputs command a speed magnitude and direction) to simplify the pilot task by automatically changing the underlying axis of control to get a consistent vehicle response. The SVC system serves as an interface between the pilot and the inner loop control system in order to allow pilots to generate these commands. The architecture enables inceptors to be mapped to outer loop control systems to produce higher level command response types, which describe the overall system response to pilot inputs. For a given command response type, pilot inputs generate a command that is limited by envelope protection and sent to the outer loop control system. An overview of the command system can be seen in Fig. 7. This section introduces the command response (Sec. III.A), envelope protection (Sec. III.B), and outer loop control (Sec. III.C) components that make up the SVC command system.

A. Command Response

The SVC concept simplifies operations (over a traditional axis-based command system) by reducing the mapping of the pitch, heave and thrust axis commands to longitudinal and vertical vector-based commands. As a result, the number of required inceptor axes is reduced from 5 to 4. The inceptor configuration utilized during this evaluation can be seen in Fig. 8. It consisted of a three axis (longitudinal, lateral, and twist) spring centered right stick and a single axis spring centered left stick.

There was also a hover button on the right stick that was used to transition to a hover mode. Two different methods of transitioning to hover were investigated in this evaluation. The first method performed a transition to hover at a nominal deceleration rate. The second method performed a transition to a commanded hover point. Figure 9 displays

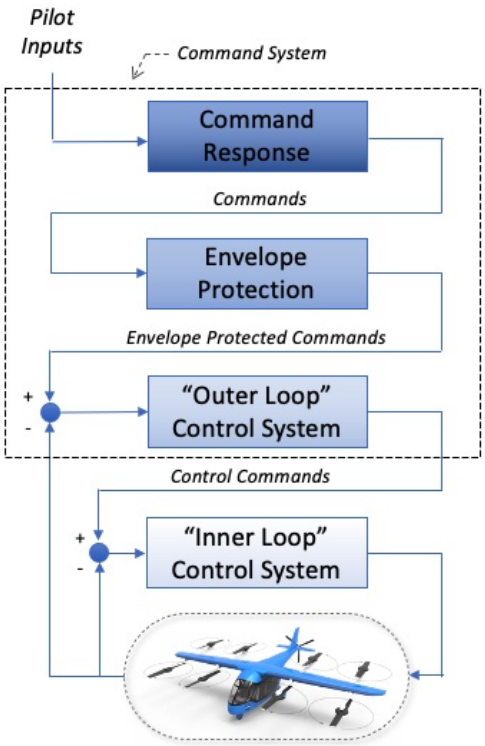

Fig. 7 Command System

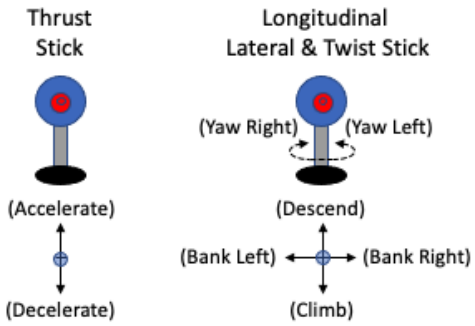

Fig. 8 Inceptor Configuration

the hover points for normal operations, transition to hover operations, and transition to a hover point operations.

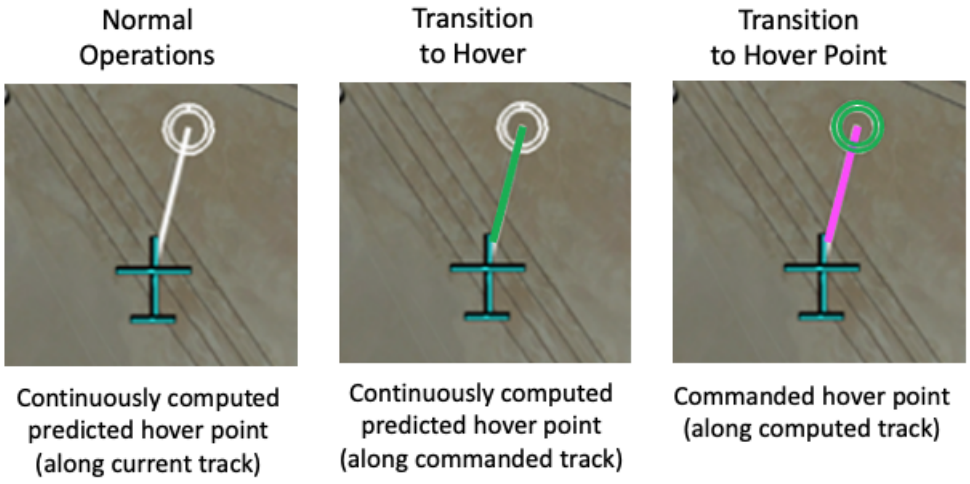

Fig. 9 Operating Modes

Under normal (non-hovering) operations, longitudinal stick inputs produced vertical speed or flight path angle (FPA) commands, thrust stick inputs produced acceleration or deceleration commands, and an automatic trim system commands pitch in the hover regime and Angle-of-Attack (AoA) in the transitional and forward flight regimes. The automatic trim system is described in Appendix VI.B. Meanwhile lateral stick and twist stick inputs continue to produce roll and yaw axis commands. The specific inceptor command response types were a function of the flight regime and groundspeed. These command response types are specified in Fig. 10.

Flight Regime	Thrust Stick	Twist Stick	Longitudinal Stick	Lateral Stick
Hover	LonVel-RC/H	Hdg-RC/H	Alt-RC/H	Bank-C/H
Transitional	Spd-RC/H	Crab-C/H / 34 KGS / Slip-C/H	34 KGS / FPA-RC/H	34 KGS / Bank-RC/H
Forward Flight				

Fig. 10 Normal Operating Command Response Types

When transitioning to hover, the vehicle commands a nominal (e.g., 2.5 knot/sec) deceleration rate, which can be overridden by applying inputs to the thrust stick. The command response types are modified to combine flight path angle and speed with track angle control, and is also fully vector commanded. This concept also drives targets comparable to setting target values in an autopilot. After decelerating below 10 knots of groundspeed, the hover mode is engaged, and thrust and lateral stick inputs will produce longitudinal and lateral groundspeed vector commands. These command response types are specified in Fig. 11.

When initiating a transition to a hover point, the predicted hover point becomes the commanded hover point. The vehicle speed and track angle are controlled to aquire and maintain a hover over that point. The command response types are modified so that thrust and lateral stick inputs will modify the longitudinal and lateral target commands, which will move the location of a command hover point with respect to the heading of the vehicle.

B. Envelope Protection

Envelope protection limits are necessary to prevent loss of control in flight (LOC-I). They are also implemented on inner rate loops so that outer angle loop limits are not exceeded. The envelope protections apply only when they are

Transition to Hover	Thrust Stick	Twist Stick	Longitudinal Stick	Lateral Stick
TRC Engaged (0-20 KGS)	LonPos-RC/H	Hdg-RC/H	Alt-RC/H	LatPos-RC/H
TRC Transition (10+ KFGS)	Spd^{Tgt}-RC/H	Crab-C/H	$Vspd^{Tgt}$-RC / FPA-H (34 KGS) / FPA^{Tgt}-RC/H	$LatVel^{Tgt}$-RC / Trk-H (34 KGS) / Trk^{Tgt}-RC/H

Fig. 11 Hover Operating Command Response Types

Transition to Hover Point	Thrust Stick	Twist Stick	Longitudinal Stick	Lateral Stick
PHC Engaged (0-20 KGS)	$LonPos^{Tgt}$-RC/H	Hdg-RC/H	Alt^{Tgt}-RC/H	$LatPos^{Tgt}$-RC/H
PHC Transition (10+ KFGS)	Spd-RC/$LonPos^{Tgt}$-H	Crab-C/H	$Vspd^{Tgt}$-RC / FPA-H (34 KGS) / FPA^{Tgt}-RC/H	$LatPos^{Tgt}$-RC/H / (34 KGS) Trk-RC / $LatPos^{Tgt}$-H

Fig. 12 Hover Point Operating Command Response Types

stricter than the performance limits which were discussed in depth in [11]. There is a distinction between standard envelope protections, some of which also apply for hover, and those tailored specifically for hover.

For RCDH:

1) limit max/min roll rate p based on max/min bank angle ϕ (from performance limits or envelope protections):

$$p_{\max_{env}} = \max\left(\dot{\phi}_{\max_{env}} - \dot{\psi}\sin\theta, \dot{\phi}_{\min_{env}} - \dot{\psi}\sin\theta\right) \quad (1)$$

$$p_{\min_{env}} = \min\left(\dot{\phi}_{\max_{env}} - \dot{\psi}\sin\theta, \dot{\phi}_{\min_{env}} - \dot{\psi}\sin\theta\right) \quad (2)$$

$$\text{with:} \quad \dot{\phi}_{\max_{env}} = \frac{1}{\tau_\phi}\left(\phi_{\max} - \phi\right) \quad \text{and} \quad \phi_{\min_{env}} = \frac{1}{\tau_\phi}\left(\phi_{\min} - \phi\right) \quad (3)$$

The limit max/min bank angle ϕ are calculated such that max/min horizontal lateral speed v_Y is not exceeded:

$$\phi_{\max_{env}} = \arcsin\left(\frac{\cos\phi}{g}\left(\dot{v}_{Y_{\max}} - \dot{v}_Y\right) + \sin\phi\right) \quad \text{with:} \quad \dot{v}_{Y_{\max}} = \frac{1}{\tau_V}\left(v_{Y_{\max}} - v_{gnd}\right) \quad (4)$$

$$\phi_{\min_{env}} = \arcsin\left(\frac{\cos\phi}{g}\left(\dot{v}_{Y_{\min}} - \dot{v}_Y\right) + \sin\phi\right) \quad \text{with:} \quad \dot{v}_{Y_{\min}} = \frac{1}{\tau_V}\left(v_{Y_{\min}} - v_{gnd}\right) \quad (5)$$

where the arcsin arguments $\left(\frac{\cos\phi}{g}\left(\dot{v}_{Y_{\max}} - \dot{v}_Y\right) + \sin\phi\right)$ and $\left(\frac{\cos\phi}{g}\left(\dot{v}_{Y_{\min}} - \dot{v}_Y\right) + \sin\phi\right)$ are limited between -1 and 1. Moreover $\phi_{\max_{env}}$ and $\phi_{\min_{env}}$ are fed through a first order lag filter to slow down their changes. The max/min horizontal lateral speed v_Y is set equal to the corresponding body fixed speed component limit in hover: $v_{Y_{\max}} = v_{b_{\max_{hov}}}$ and $v_{Y_{\min}} = v_{b_{\min_{hov}}}$. Furthermore the horizontal lateral acceleration $\dot{v}_Y$ is calculated as follows: $\dot{v}_Y = \dot{v}_b\cos\phi - \dot{w}_b\sin\phi$ with $\dot{v}_b = \left(n_y + \cos\theta\sin\phi\right)g + pw_b - ru_b$ and $\dot{w}_b = \left(n_z + \cos\theta\cos\phi\right)g + qu_b - pv_b$. The derivation of Eq. (4),(5) is given in [11].

2) limit maximum acceleration/deceleration:

$$\dot{V}_{\max_{env}} = \min\left(\dot{V}_{CAS_{\max}}, \frac{1}{\tau_V}\left(V_{CAS_{\max}} - V_{CAS_{comp}}\right)\right) \quad (6)$$

$$\dot{V}_{\min_{env}} = \max\left(\dot{V}_{CAS_{\min}}, \frac{1}{\tau_V}\left(V_{CAS_{\min}} - V_{CAS_{comp}}\right)\right) \quad (7)$$

Custom values for the computed calibrated airspeed $V_{CAS_{comp}}$ are used here. More details are given in Eq. (**??**) – (**??**).

Limits for flight path angle γ and vertical speed $\dot{h}$:
For RCHH: limit flight path angle γ (only when groundspeed V_{gnd} exceeds certain threshold, not in hover):

$$\gamma_{\max_{\text{env}}} = \arctan \frac{\dot{h}_{\max}}{V_{\text{gnd}}} \tag{8}$$

$$\gamma_{\min_{\text{env}}} = \arctan \frac{\dot{h}_{\min}}{V_{\text{gnd}}} \tag{9}$$

For speed engaged:

$$\gamma_{\max_{\text{env}}} = \min\left(\gamma_{\max_{\text{ctl}}}, \gamma_{V_{\text{CAS}}+10\text{kts}}, \gamma_{V_{\text{cmd}}}\right) \tag{10}$$

$$\gamma_{\min_{\text{env}}} = \min\left(\gamma_{\min_{\text{ctl}}}, -\gamma_{V_{\text{CAS}}-10\text{kts}}, -\gamma_{V_{\text{cmd}}}\right) \tag{11}$$

For ACSH:

$$\gamma_{\max_{\text{env}}} = \min\left(\gamma_{\max_{\text{ctl}}}, \gamma_{V_{\text{CAS}}+5\text{kts}}\right) \tag{12}$$

$$\gamma_{\min_{\text{env}}} = \min\left(\gamma_{\min_{\text{ctl}}}, -\gamma_{V_{\text{CAS}}-5\text{kts}}\right) \tag{13}$$

For all other modes:

$$\gamma_{\max_{\text{env}}} = \min\left(\gamma_{\max_{\text{ctl}}}, \gamma_{V_{\text{CAS}_{\min}}}\right) \tag{14}$$

$$\gamma_{\min_{\text{env}}} = \min\left(\gamma_{\min_{\text{ctl}}}, -\gamma_{V_{\text{CAS}_{\max}}}\right) \tag{15}$$

Subsequently:

$$V_{Z_{\max}} = \tan\gamma_{\max} \cdot V_{\text{gnd}} \tag{16}$$

$$V_{Z_{\min}} = \tan\gamma_{\min} \cdot V_{\text{gnd}} \tag{17}$$

after which $\gamma_{\max_{\text{env}}}$ and $\gamma_{\min_{\text{env}}}$ as well as $V_{Z_{\max}}$ and $V_{Z_{\min}}$ are fed through a first order lag filter to slow down their changes. In Eq. (10)–(15), the quantities $\gamma_{V_\bullet}$ are flight path angles based on a certain calibrated target speed. They are calculated as follows:

$$\gamma_{V_\bullet} = \arcsin\left(\sin\gamma - \frac{\dot{V}_{\text{TAS}_{\text{cmd}}} - \dot{V}_{\text{TAS}}}{g}\right) \tag{18}$$

where the arcsin argument $\left(\sin\gamma - \frac{\dot{V}_{\text{TAS}_{\text{cmd}}} - \dot{V}_{\text{TAS}}}{g}\right)$ is limited between -1 and 1. $\dot{V}_{\text{TAS}_{\text{cmd}}}$ consists of a limited term that is based on a limited speed error $\dot{V}_{\Delta V}$ and an additional term that compensates for thrust based speed acceleration or deceleration limits, and which differs for climb and descent:

$$\dot{V}_{\text{TAS}_{\text{cmd}}} = \dot{V}_{\Delta V} - X_{u_{\delta_{\text{thr}}}}(1 - \delta_{\text{thr}}) \quad \text{for climb} \tag{19}$$

$$\dot{V}_{\text{TAS}_{\text{cmd}}} = \dot{V}_{\Delta V} + X_{u_{\delta_{\text{thr}}}}\delta_{\text{thr}} \quad \text{for descent} \tag{20}$$

where $X_{u_{\delta_{\text{thr}}}}$ is the coefficient that calculates the impact of a throttle change on the forward speed component. Moreover, $\dot{V}_{\Delta V}$ is limited between the previously defined $\dot{V}_{\min_{\text{env}}}$ and $\dot{V}_{\max_{\text{env}}}$ (see Eq. (6)–(7)) and where:

$$\dot{V}_{\Delta V} = \frac{1}{\tau_V}\Delta_V + \varepsilon_{\text{corr}_{\text{IAS}\to\text{TAS}}} \tag{21}$$

where $\varepsilon_{\text{corr}_{\text{IAS}\to\text{TAS}}}$ is a correction term for the conversion from indicated airspeed (IAS, with which the target is defined) to true airspeed (TAS, with which the flight path angle is calculated). The limited speed error ΔV itself is calculated as follows:

$$\Delta V = V_{\text{TAS}_{\text{target}}} - V_{\text{TAS}} \tag{22}$$

which is also limited between $\dot{V}_{\text{CAS}_{\min}} \cdot \tau_V$ and $\dot{V}_{\text{CAS}_{\max}} \cdot \tau_V$.
Limits for pitch attitude angle θ, pitch rate q and the flight path angular rate $\dot{\gamma}$:

1) For TBL/STBL: limit max/min pitch attitude angle θ based on max/min airspeed V_{CAS} (also in hover):

$$\theta_{\mathrm{max_{env}}} = \arcsin\left(\sin\theta - \frac{\left(\dot{V}_{\mathrm{CAS_{min}}} - \dot{V}_{\mathrm{CAS_{comp}}}\right)\cos\theta}{g}\right) \quad \text{with:} \quad \dot{V}_{\mathrm{CAS_{min_{env}}}} = \max\left\{\frac{1}{\tau_V}\left(V_{\mathrm{CAS_{min}}} - V_{\mathrm{CAS_{comp}}}\right), \dot{V}_{\mathrm{CAS_{min_{perf}}}}\right\} \tag{23}$$

$$\theta_{\mathrm{min_{env}}} = \arcsin\left(\sin\theta - \frac{\left(\dot{V}_{\mathrm{CAS_{max}}} - \dot{V}_{\mathrm{CAS_{comp}}}\right)\cos\theta}{g}\right) \quad \text{with:} \quad \dot{V}_{\mathrm{CAS_{max_{env}}}} = \min\left\{\frac{1}{\tau_V}\left(V_{\mathrm{CAS_{max}}} - V_{\mathrm{CAS_{comp}}}\right), \dot{V}_{\mathrm{CAS_{max_{perf}}}}\right\} \tag{24}$$

The computed calibrated airspeed $V_{\mathrm{CAS_{comp}}}$ and its time derivative $\dot{V}_{\mathrm{CAS_{comp}}}$ are used here, such that these equations also hold in hover. For the derivation of Eq. (23),(24), see [11].

2) For speed engaged / ACSH:

$$\theta_{\mathrm{max_{env}}} = \min\left(\theta_{\mathrm{max_{ctl}}}, \alpha + \gamma_{\mathrm{max_{env}}}\right) \tag{25}$$

$$\theta_{\mathrm{min_{env}}} = \max\left(\theta_{\mathrm{min_{ctl}}}, \alpha + \gamma_{\mathrm{min_{env}}}\right) \tag{26}$$

where $\gamma_{\mathrm{max_{env}}}$ and $\gamma_{\mathrm{min_{env}}}$ come from Eq. (10)–(13).

3) For all other modes:

$$\theta_{\mathrm{max_{env}}} = \theta_{\mathrm{max_{ctl}}} \tag{27}$$

$$\theta_{\mathrm{min_{env}}} = \theta_{\mathrm{min_{ctl}}} \tag{28}$$

Limit max/min pitch rate q based on max/min pitch attitude angle θ via $\dot{\theta}$:

$$\dot{\theta}_{\mathrm{max_{env}}} = \min\left(\dot{\theta}_{\mathrm{max_{ctl}}}, \frac{1}{\tau_\theta}\left(\theta_{\mathrm{max_{env}}} - \theta\right)\right) \tag{29}$$

$$\dot{\theta}_{\mathrm{min_{env}}} = \max\left(\dot{\theta}_{\mathrm{min_{ctl}}}, \frac{1}{\tau_\theta}\left(\theta_{\mathrm{min_{env}}} - \theta\right)\right) \tag{30}$$

$$q_{\mathrm{max_{env}}} = \max\left(\left(\dot{\theta}_{\mathrm{max_{env}}}\cos\phi + \dot{\psi}\sin\phi\cos\theta\right), \left(\dot{\theta}_{\mathrm{min_{env}}}\cos\phi + \dot{\psi}\sin\phi\cos\theta\right)\right) \tag{31}$$

$$q_{\mathrm{min_{env}}} = \min\left(\left(\dot{\theta}_{\mathrm{max_{env}}}\cos\phi + \dot{\psi}\sin\phi\cos\theta\right), \left(\dot{\theta}_{\mathrm{min_{env}}}\cos\phi + \dot{\psi}\sin\phi\cos\theta\right)\right) \tag{32}$$

Limit flight path angular rate $\dot{\gamma}$ with information from above:

$$\dot{\gamma}_{\mathrm{max_{env}}} = \min\left(\min\left(\dot{\gamma}_{\mathrm{max_{ctl}}}, \tau_\gamma\left(\gamma_{\mathrm{max_{env}}} - \gamma\right)\right), \dot{\theta}_{\mathrm{max_{env}}}\right) \tag{33}$$

$$\dot{\gamma}_{\mathrm{min_{env}}} = \max\left(\max\left(\dot{\gamma}_{\mathrm{min_{ctl}}}, \tau_\gamma\left(\gamma_{\mathrm{min_{env}}} - \gamma\right)\right), \dot{\theta}_{\mathrm{min_{env}}}\right) \tag{34}$$

For heading rate, in RCDH:

$$\dot{\psi}_{\mathrm{max_{env}}} = \max\left(\frac{q_{\max}\sin\phi + r_{\max}\cos\phi}{\cos\theta_{\mathrm{lim}}}, \frac{q_{\min}\sin\phi + r_{\min}\cos\phi}{\cos\theta_{\mathrm{lim}}}\right) \tag{35}$$

$$\dot{\psi}_{\mathrm{min_{env}}} = \min\left(\frac{q_{\max}\sin\phi + r_{\max}\cos\phi}{\cos\theta_{\mathrm{lim}}}, \frac{q_{\min}\sin\phi + r_{\min}\cos\phi}{\cos\theta_{\mathrm{lim}}}\right) \tag{36}$$

Else:

$$\dot{\psi}_{\mathrm{max_{env}}} = \frac{g\tan\phi_{\max}}{V_{\mathrm{TAS_{lim}}}\cos\theta_{\mathrm{lim}}} \tag{37}$$

$$\dot{\psi}_{\mathrm{min_{env}}} = \frac{g\tan\phi_{\min}}{V_{\mathrm{TAS_{lim}}}\cos\theta_{\mathrm{lim}}} \tag{38}$$

The Appendices in [11] derive Eq. (37),(38). These limits are first order filtered to slow down their changes. The denominators $\cos\theta_{\mathrm{lim}}$ in Eq. (35)–(38) and $V_{\mathrm{TAS_{lim}}}$ in Eq. (37),(38) are singularity protected as follows:

$$V_{\mathrm{TAS_{lim}}} = \max\left(V_{\mathrm{TAS}}, 10\ \mathrm{kts}\right) \tag{39}$$

$$\cos\theta_{\mathrm{lim}} = \mathrm{sgn}\left(\cos\theta\right)\max\left(|\cos\theta|, 0.005\right) \tag{40}$$

The time constants τ_ϕ, τ_V, τ_θ and τ_ψ are defined consistently with these used by the autopilot.

C. Outer Loop Control

For a given command response type, pilot inputs generate command response outputs for the outer loop control system. The outer loop control system is responsible for mapping the outer loop responses to the necessary inputs for the inner loop control system, which is dependent on the flight regime and thus inner loop control modes (as seen in Fig. 5). In some cases it is necessary to convert from an angle command to an angular rate or from earth to body fixed commands (or vice versa), and sometimes both are needed for blending. The following section describes these transformations. Fig. 13 shows the outer loop control architecture, specifically how the individual outer loop control systems (rectangles) are interconnected and connected to the inner loop control systems (ovals). There are 16 different outer loop control systems, which are all explained in Appendix VI.D.

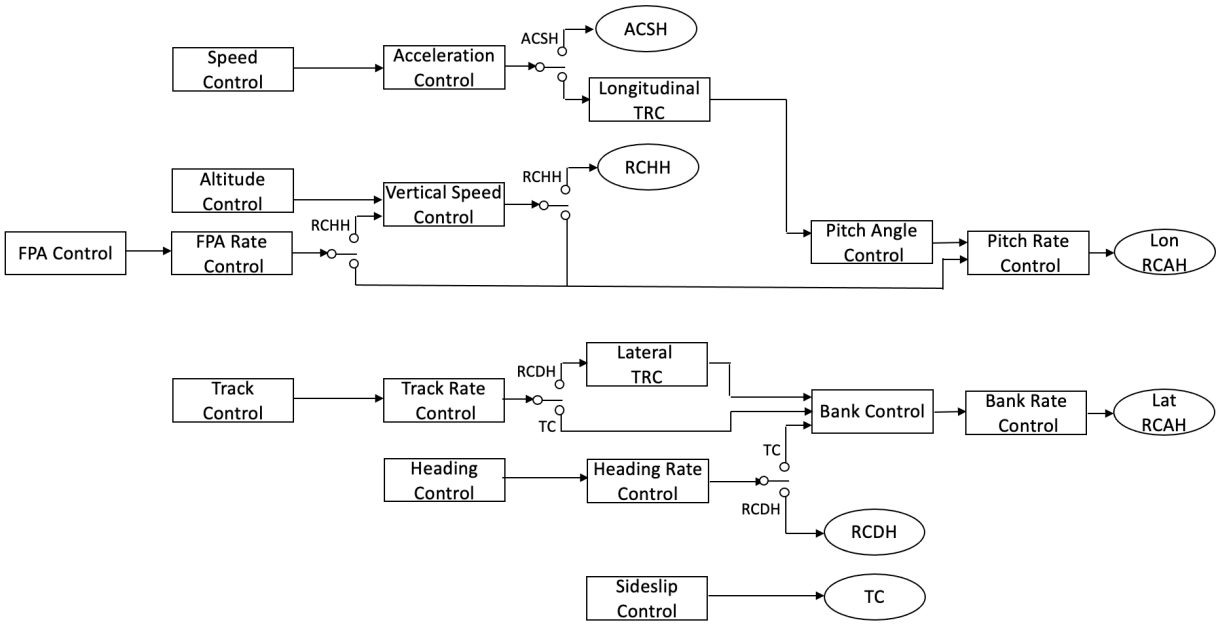

Fig. 13 Outer Loop Control Architecture

IV. Preliminary Results

Simulation evaluations focused on performing flight test maneuvers to evaluate the handling qualities of the LPC under the SVC concept under varying environmental and operational conditions. These preliminary results focus on the transition from approach to hover, highlighting challenges in dissipating energy to prepare for landing. These preliminary evaluations were performed in a desktop simulation environment with repeatable automation flying an approach to landing maneuver. Final results will include piloted simulator evaluations of both approach to hover and the hover operation concepts under varying environmental (wind), operational (glidepath angle, deceleration rates) and display information.

A. ACEL-RATE Lab

The Aerospace Cognitive Engineering Lab – Rapid Automation Test Environment (ACEL-RATE) simulator is a fixed-based flight simulation facility which was used for testing, development and validation. The system, shown in Fig. 14), consists of wide-view outside visual display, three primary displays, two chin-window displays, and reconfigurable cockpit hardware (currently in a two stick inceptor configuration, as defined in Fig. 8). The Out-the-Window is a 200-degree field of view screen which runs a customized visual database built in RSI [21].

(a) Simulator facility (b) Pilot station

Fig. 14 ACEL-RATE simulator

B. Heliport Approach Transition to Hover Maneuver

This maneuver builds on the previous development of a heliport approach, but is designed to focus on the transition from approach to hover. The previous heliport approach, described in detail in [10], was based on a combination of the ADS-33E Decelerating approach, previous Powered Lift approach research [22] and collaboration on UAM Heliport approach procedures [23, 24]. While that maneuver included an initial lateral and vertical glidepath capture, this approach transition maneuver initializes on the glideslope. This allows the task to focus on the deceleration and transition for landing. Additionally, while the previous maneuver terminated at the crossing of the final approach and takeoff area (FATO), this approach includes a transition to stabilized hover and landing over the desired landing location, allowing evaluation on the hover and landing task. Specifically, pilot determination of when to begin the deceleration can be explored, under varying operational and environmental conditions.

For these preliminary results, this maneuver is conducted at three different potential glidepath angles : 6, 9 and 12degrees. A maximum allowable deceleration rate is also varied to explore the control strategy performance with varying aggressiveness. A transition to hover (TRC) is armed and engaged at 30knots. These tests are performed in light turbulence with a 17knot crosswind.

C. Discussion of Results

Fig. 15 gives an overview of the three different flight path angles and two different deceleration rates. These two figures show altitude above ground level (AGL) in ft and calibrated airspeed (CAS) in kts as a function of the distance

to the vertiport landing zone in ft, with the end point at the right side of the graph. The altitude plot shows the three different flight path angles of 6 (nominal), 9 and 12degrees. There are two deceleration rates for each angle, namely -1.5 and -2.5kts/s. The speed graph shows the two different deceleration rates resulting in two different slopes in the deceleration phases. Different flight path angles result in different starting speeds on the glideslope: 70kts for 6deg, 60kts for 9deg and 45kts for 12deg.

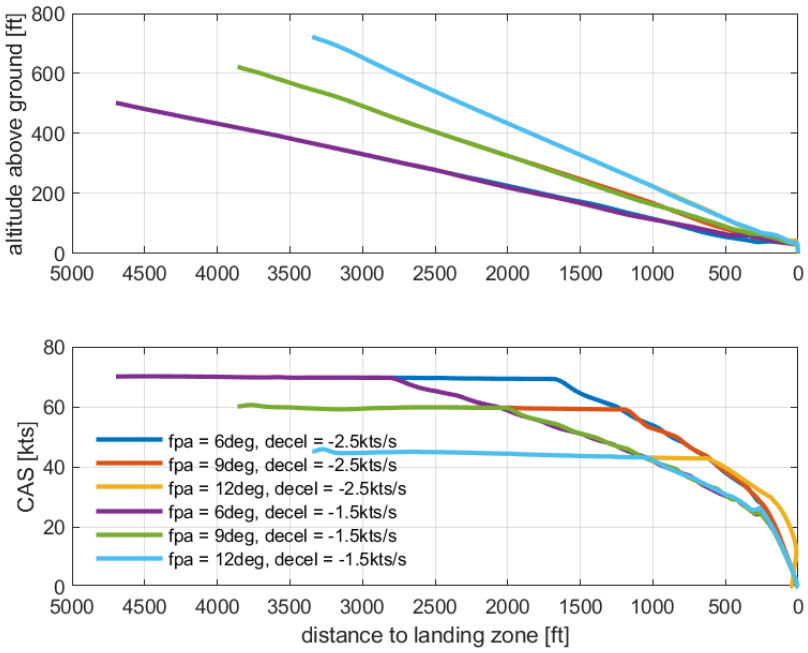

Fig. 15 Altitude and speed profile along track distance to touchdown point for various glideslope angles and deceleration rates

Fig. 16 shows the control action over time on an axis allocation level. Fig. 16(a) shows the allocation of the total control action over the different control axes namely longitudinal δ_{lon} (pitch), lateral δ_{lat} (roll), collective δ_{col} (vertical) and pedals δ_{ped} (yaw). All allocation ranges are normalized towards a -1 to +1 scale. The different scenarios result in similar control action allocation over the axes overall, and show satisfactory margin to saturation for most of the axes. Only the collective reaches the saturation limits. The -1 limit in the beginning of some scenarios corresponds to the rotors not having to provide any significant net upward vertical force in this higher speed flight phase. They do for the two 12deg glideslope and 45kts CAS (lowest speed) scenarios. In all fast deceleration scenarios, there is a very brief instantaneous saturation of the collective on the upper limit +1 during the transition. The slow deceleration scenarios of -1.5kts/s do not reach this limit, although the most gradual glideslope of 6deg comes very close. This signifies that the angle of attack or pitch attitude angle (depending on which flight phase) cannot be reduced as much as intended to. Fig. 16 shows the control action on the throttle for deceleration. The throttle range is normalized towards a 0 to +1 scale. The spread in initial throttle settings early in the scenarios corresponds to the different speed regimes. In all scenarios, the throttle hits the minimum limit of 0 at some point during the approach, which illustrates that the vehicle reaches its maximum deceleration limit.

Fig. 17 shows how the total control action at the control effector side is distributed over the control surfaces in Fig. 17(a) on one side and the individual lifting rotors in Fig. 17(b) on the other. As the speed is reducing and the vehicle is transitioning towards hover mode, the control surfaces are blending out and the lifting rotors are ramping up. In Fig. 17(a), only the left aileron action is shown, because the right aileron action is anti-symmetric. The maximum deflection limits are respectively 30deg, 15deg and 30deg for aileron, elevator and rudder. No saturation limits are reached for any control surface, but ailerons and elevators have significantly more margin to saturation compared to the rudder. This is because of the 17kts crosswind which needs directional compensation. Most scenarios exhibit similar trends in the control surface action, and the spread in initial elevator deflections early in the scenarios corresponds to the different

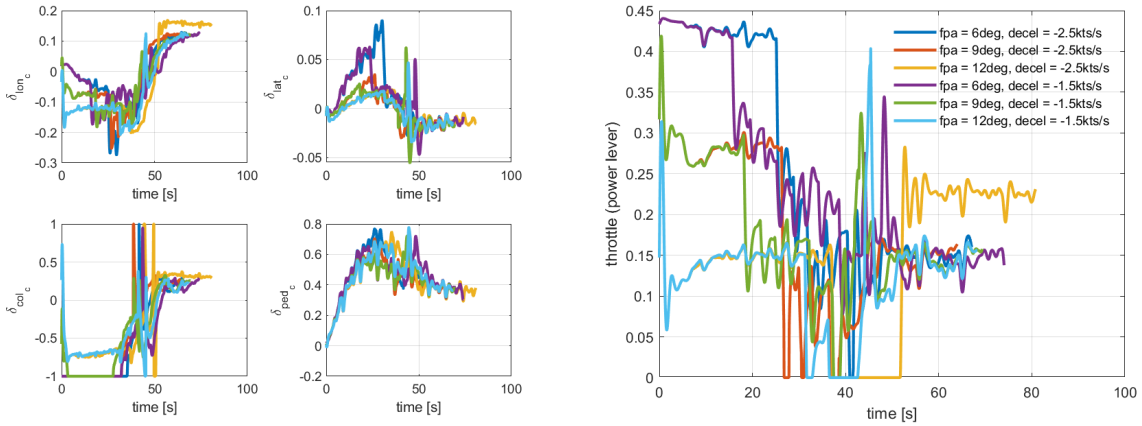

(a) Allocation over control axes

(b) Throttle

Fig. 16 Allocations on control axes and throttle for various glideslope angles and deceleration rates

speed regimes, similar like for the throttle in Fig. 16(b). The individual rotor actions are shown in Fig. 17(b). Again, one can observe similar trends for the different scenarios. Initial control action early in the scenarios shows that yaw control is by the rudder is augmented with differential torque provided by the rotors no. 1, 3, 6 and 8 deflecting their blade angles further than rotors no. 2, 4, 5 and 7. Overall, the rotors provide more thrust-borne lift as the wing-borne lift is gradually reducing with the airspeed. The initial nonzero collective action early in the scenarios with the lower airspeeds in Fig. 16(a) results in nonzero blade angle deflection for rotors no. 2, 4, 5 and 7, in contrast to the other higher airspeed scenarios.

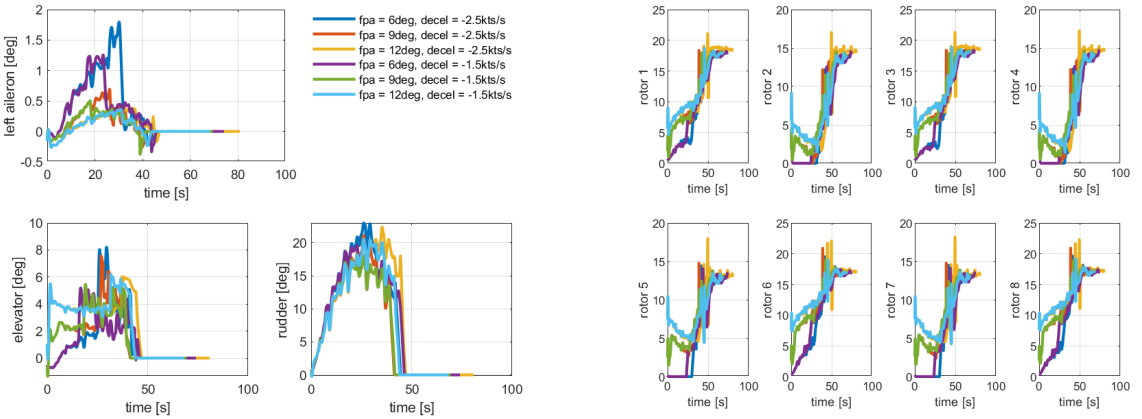

(a) Control surface actuators

(b) Rotor actuators

Fig. 17 Control surface and rotor actuator commands for various glideslope angles and deceleration rates

Fig. 18 shows time histories for angle of attack α and pitch attitude angle θ during the approach scenarios. Angle of attack is not shown for speed regimes where CAS drops below 10kts as aerodynamic angles have no practical meaning there. Overall trends are similar across all scenarios, and it is shown that the control concept is successful in protecting α and θ from exceeding their safe envelope limits of 18deg and 10deg respectively.

Fig. 19 shows total energy management during the approach for all scenarios with different energy dissipation rates for glideslope (change in potential energy (PE)) as well as rate of deceleration (reduction in kinetic energy (KE)). These

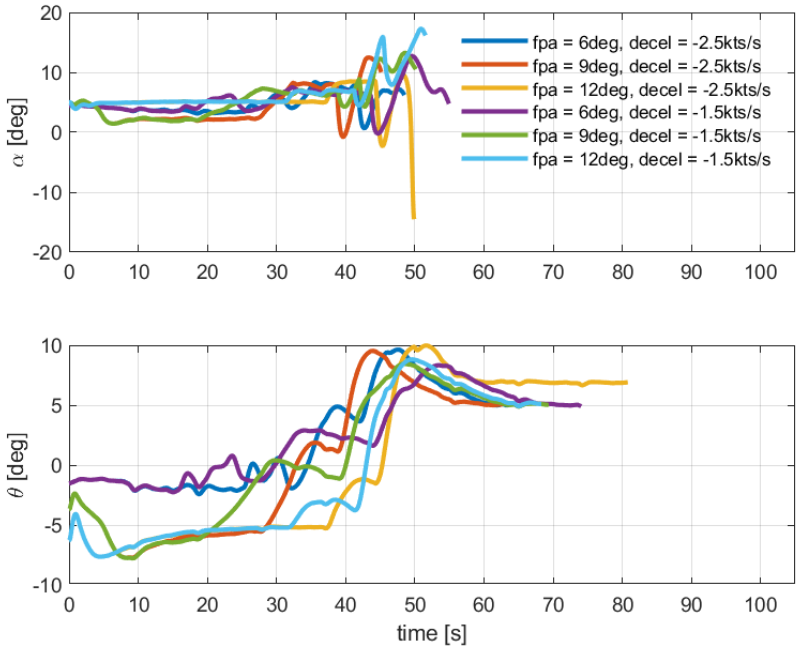

Fig. 18 Angle of attack and pitch attitude angle for various glideslope angles and deceleration rates)

figures show specific energy levels, which means that they are independent of the vehicle mass. Fig. 19(a) emphasizes the rate of energy dissipation along track towards the landing zone. Potential energy only (PE) is shown by the dashed lines and total energy (PE+KE) by the solid lines. The maximum slope of the solid lines illustrates the maximum dissipation rate of total energy during the approach. While the three slower deceleration scenarios show a wider spread in total energy dissipation rates by means of their slopes in the final phase, the three faster deceleration scenarios manifest a narrower spread in slopes and thus energy dissipation rates. This figure also exhibits which approach is the most demanding from an energy dissipation perspective (steepest descent and fastest deceleration rate). Fig. 19(b) compares the changes in potential versus kinetic energy. This illustrates the transition from change in potential energy only (descent at constant speed), versus simultaneous change in potential and kinetic energy (decelerating descent) where both reduce at a constant ratio. A slower deceleration results in a more gradual change in kinetic energy. The steepest descent with the slowest deceleration comes closest to an energy dissipation ratio of one-to-one where one needs to dissipate almost as much potential as kinetic energy.

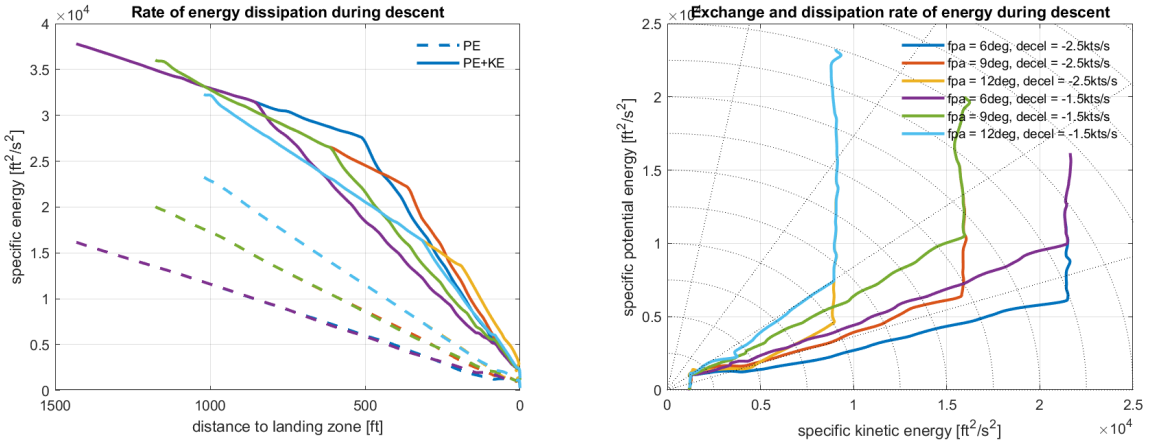

(a) Along track distance

(b) Potential vs kinetic

Fig. 19 Total mechanical energy dissipation for various glideslope angles and deceleration rates

V. Summary and Conclusions

This study focused on the development of a simplified vehicle control concept specifically designed for a lift-plus-cruise eVTOL vehicle with collective controls. Preliminary evaluations focused on autoflight mode flown approaches with different glideslopes and deceleration rates. Control allocation and saturation as well as energy management have been studied. Future work will include among others various kinds of wind and gust disturbance rejection, and manually flown approaches in the ACEL-RATE lab as well as the Vertical Motion Simulator.

Acknowledgments

The authors wish to thank the Airspace Operations and Safety Program's Advanced Air Mobility project and FAA agreement 692M15-19-N-00010 for funding this work. The authors would like to acknowledge Loran Haworth, John Archdeacon, Nelson Iwai and Amber Villa. Finally, many FAA colleagues were instrumental during the course of this project, namely Ross Schaller, Dave Sizoo, Mitch Soth, John Jordan and David Webber.

VI. Appendices

A. Inner Loop Control Modes

The inner loop control system corresponding to each mode generally consists of a reference model and an error controller. This setup allows for decoupling of the gain tuning according to the purpose. The gains in the reference model serve for command shaping, i.e. the responsiveness of the vehicle to a commanded input. The PID gains of the error controller tune how quick disturbances (such as turbulence induced deviations) are compensated for.

Acceleration Command Speed Hold (ACSH) This acceleration command system is basically a pure integral action based linear controller that makes use of the error between the commanded speed rate of change $\dot{V}_{\text{cmd}}$ and the computed calibrated airspeed rate of change $\dot{V}_{\text{CAS}_{\text{comp}}}$ for calculating the required linear acceleration for the dynamic inversion loop:

$$\dot{u}_{\text{req}} = \dot{V}_{\text{ref}} = \frac{1}{\tau_u}\left(\dot{V}_{\text{cmd}} - \dot{V}_{\text{CAS}_{\text{comp}}}\right) dt \tag{41}$$

This computed calibrated airspeed rate of change is scheduled in hover according to the speed range. Outside hover and in hover but above 40 kts groundspeed, it is basically the actual calibrated airspeed rate of change. This does not work for lower speeds due to wind and turbulence. For lower speeds, it is first scheduled towards groundspeed rate of change and next to forward groundspeed rate of change. Below 10 kts it is exactly the forward groundspeed rate of change.

Angle of Attack Command (AOAC) The Angle Of Attack Command module (AOAC) basically calculates a commanded body fixed vertical speed w_{cmd}, based on the maximum allowed angle of attack α_{max} and the body fixed foward speed u_b:

$$w_{\text{cmd}} = \tan\alpha_{\text{max}} \cdot u_b \tag{42}$$

This maximum angle of attack α_{max} value can change depending on the flight regime. Next, this commanded vertical speed w_{cmd} is fed through its respective rate command module as discussed in Fig. 6, resulting in a required vertical acceleration $\dot{w}_{\text{req}}$, to be fed to the respective dynamic inversion calculation.

Rate Command Attitude Hold (RCAH) Rate Command Attitude Hold is a variation of ACAH, where the commanded inputs are body fixed roll and pitch rates p_{cmd} and q_{cmd}. This mode is used in the cruise forward flight phase. This command shaping consists of a first order reference model with the corresponding time constant τ_{ref}. This reference model is connected to a linear PI controller. The angular and linear accelerations from the first order reference model $\dot{p}_{\text{ref}}$ and $\dot{q}_{\text{ref}}$ are fed forward and added to the linear controller output to minimize lag between response and reference signal. Required body angular accelerations $\dot{p}_{\text{req}}$ and $\dot{q}_{\text{req}}$ are the output of the linear controller, to be fed to the dynamic inversion calculation. Fig. 6 illustrates the interconnections between commanded inputs, reference model and controller for this control mode.

Subsequent modes, such as Rate Command Direction Hold (RCDH), Rate Command Height Hold (RCHH), Angle Of Attack Command (AOAC) and Turn Coordination (TC) have a similar setup as RCAH, but then with the controlled variables body fixed yaw rate r_{cmd} and vertical speed w_{cmd}, as also shown in Fig. 6, supplemented by a few additional coordinate transformations as elaborated in the paragraphs below.

Rate Command Direction Hold (RCDH) Rate Command Direction Hold is similar to RCAH. A steady commanded earth referenced yaw rate commands a steady rate of change of the heading. This mode is used in the hover and landing phases of flight.

In this case the commanded input is the earth referenced rate of change of the heading $\dot{\psi}_{\text{cmd}}$, which is transformed in a commanded body fixed yaw rate r_{cmd}, based on the following inverse Euler equation:

$$r_{\text{cmd}} = \dot{\psi}_{\text{cmd}} \cos\theta \cos\phi - \dot{\theta}\sin\phi \tag{43}$$

Next, this commanded yaw rate r_{cmd} is fed through its respective rate command module as discussed in Fig. 6, resulting in a required yaw angular acceleration $\dot{r}_{\text{req}}$, to be fed to the dynamic inversion calculation.

Rate Command Height Hold (RCHH) Rate Command Height Hold is similar to the both previous ones. A steady height rate command results in a steady climb or sink rate. This mode is used in lower speed flight regimes.

In this case, the commanded input is the earth referenced height rate of change $\dot{h}_{\text{cmd}}$, which is transformed in a commanded body fixed vertical speed component w_{cmd} as follows:

$$w_{\text{cmd}} = \frac{1}{\cos\phi\cos\theta}\left(-\dot{h}_{\text{cmd}} + \sin\theta \cdot u_b + \sin\phi\cos\theta \cdot v_b\right) \tag{44}$$

Next, this commanded vertical speed w_{cmd} is fed through its respective rate command module as discussed in Fig. 6, resulting in a required vertical acceleration $\dot{w}_{\text{req}}$, to be fed to the dynamic inversion calculation.

For the feedback path in the linear controller, one needs to compute the vertical speed in body axes from vertical speed in earth fixed axes (to incorporate vertical winds, etc.)

$$w_b = \frac{1}{\cos\phi\cos\theta}\left(\dot{z} + \sin\theta \cdot u_b + \sin\phi\cos\theta \cdot v_b\right) \tag{45}$$

Turn Coordination (TC) For turn coordination, sideslip β control has been implemented as outer loop over rate control according to the following control law:

$$r_{\text{cmd}} = -K_\beta\left(\beta_{\text{cmd}} - \beta\right) + r_{\text{TC}} \tag{46}$$

where the controller gain $K_\beta = \frac{\omega_r}{3}$. In Eq. 46, yaw rate for turn coordination r_{TC} is calculated as follows:

$$r_{\text{TC}} = \sin\phi\cos\theta \cdot \frac{g_0}{V_{\text{TAS}_{\text{lim}}}} \tag{47}$$

where the denominator $V_{\text{TAS}_{\text{lim}}}$ is singularity protected as follows:

$$V_{\text{TAS}_{\text{lim}}} = \max\left(V_{\text{TAS}}, 10\text{ kts}\right) \tag{48}$$

Next, this commanded yaw rate r_{cmd} is fed through its respective rate command module as discussed in Fig. 6, resulting in a required yaw angular acceleration $\dot{r}_{\text{req}}$, to be fed to the dynamic inversion calculation.

B. Automatic Trim

Automatic trim is used to enhance the acceleration and deceleration rate of the vehicle, by taking advantage of the additional axis of control. The automatic trim commands pitch in the hover regime, and angle of attack (i.e., using heave) in the transitional regime.

Angle of Attack Trim For angle of attack trim, a commanded angle of attack α is calculated that corresponds to a given normalized thrust setting, according to the following mapping:

$$\alpha_{\text{cmd}} = \left(\alpha_{\text{min}} - \alpha_{\text{max}}\right)\delta_{\text{thr}} + \alpha_{\text{max}} \tag{49}$$

where $\alpha_{\text{min}} = 0deg$ and $\alpha_{\text{max}} = 10deg$ and δ_{thr} is the normalized thrust setting, between 0 and 1. Subsequently, this command is sent through a first order filter that serves as reference model:

$$\dot{\alpha}_{\text{ref}} = \frac{1}{\tau_\alpha}\left(\alpha_{\text{cmd}} - \alpha_{\text{ref}}\right) \tag{50}$$

The resulting angle of attack command is sent to the Angle of Attack Command (AOAC) inner-loop control system.

Pitch Trim For pitch trim, a pitch attitude angle θ is calculated that corresponds to a given normalized thrust setting, according to the following mapping:

$$\theta_{\text{cmd}} = \left(\theta_{\text{min}} - \theta_{\text{max}}\right)\delta_{\text{thr}} + \theta_{\text{max}} \tag{51}$$

where $\theta_{\text{min}} = 0deg$ and $\theta_{\text{max}} = 10deg$ and δ_{thr} is the normalized thrust setting, between 0 and 1. Subsequently, this command is sent through a first order filter that serves as reference model:

$$\dot{\theta}_{\text{ref}} = \frac{1}{\tau_\theta}\left(\theta_{\text{cmd}} - \theta_{\text{ref}}\right) \tag{52}$$

The resulting pitch angle command is sent to the Pitch Angle Control outer-loop control system.

C. Command Response Types

Command response types describe the overall system response to pilot inputs. There are 16 different outer loop control systems introduced in Fig. 13, which are explained below. They are broken down by category:

- State Command State Hold
- State Rate Command State Hold
- Target Rate Command Target Hold

1. State Command State Hold

In this category of command response, a constant inceptor deflection results in a constant commanded state. Releasing the inceptor back to the neutral position results in a zero (or nominal) commanded state. Pilot inputs are scaled over the allowable range of the commanded state. Subsequently, this command is fed through a first-order lag filter with a time constant that serves as a reference model. A high level description of the command response types that fit under this category are described below.

Bank-C/H For Bank Command / Bank Hold, a constant inceptor deflection results in a constant commanded bank angle. Releasing the inceptor back to the neutral position results in a zero commanded bank angle. The bank angle command is sent to the Bank Control outer-loop control system.

Crab-C/H For Crab Command / Crab Hold, a constant inceptor deflection results in a constant commanded crab angle. Releasing the inceptor back to the neutral position results in a zero commanded crab angle. The crab angle command is converted to a sideslip command and sent to the Sideslip Control outer-loop control system.

Slip-C/H For Slip Command / Slip Hold, a constant inceptor deflection results in a constant commanded sideslip angle. Releasing the inceptor back to the neutral position results in a zero commanded sideslip angle. The sideslip angle command is sent to the Sideslip Control outer-loop control system.

2. State Rate Command State Hold

In this category of command response, a constant inceptor deflection results in a constant commanded rate of change in the aircraft state. Releasing the inceptor back to the neutral position results in a zero rate command to maintain the current state through integrators in the inner-loop control system (II.B.2). Pilot inputs are scaled over the allowable range of the commanded rate of change. A high-level description of the command response types that fit under this category are described below.

Alt-RC/H For Altitude Rate Command / Altitude Hold, a constant inceptor deflection results in a constant commanded altitude rate (i.e., vertical speed). Releasing the inceptor back to the neutral position results in a zero altitude rate command to maintain the current altitude. The altitude rate command is sent to the Vertical Speed Control outer-loop control system.

Bank-RC/H For Bank Rate Command / Bank Hold, a constant inceptor deflection results in a constant commanded bank rate. Releasing the inceptor back to the neutral position results in a zero bank rate command to maintain the current bank angle. The bank rate command is sent to the Bank Rate Control outer-loop control system.

Fpa-RC/H For Flight Path Angle Rate Command / Flight Path Angle Hold, a constant inceptor deflection results in a constant commanded flight path angle rate. Releasing the inceptor back to the neutral position results in a zero flight path angle rate command to maintain the current flight path angle. The flight path angle rate command is sent to the FPA Rate Control outer-loop control system.

Hdg-RC/H For Heading Rate Command / Heading Hold, a constant inceptor deflection results in a constant commanded heading rate. Releasing the inceptor back to the neutral position results in a zero heading rate command to maintain the current heading angle. The heading rate command is sent to the Heading Rate Control outer-loop control system.

LatPos-RC/H For Lateral Position Rate Command / Lateral Position Hold, a constant inceptor deflection results in a constant commanded lateral rate (i.e., ground relative lateral velocity). Releasing the inceptor back to the neutral position results in a zero lateral rate command to maintain the current lateral position. The lateral rate command is sent to the lateral component of the Translational Rate Control outer-loop control system.

LonPos-RC/H For Longitudinal Position Rate Command / Longitudinal Position Hold, a constant inceptor deflection results in a constant commanded longitudinal rate (i.e., ground relative longitudinal velocity). Releasing the inceptor back to the neutral position results in a zero longitudinal rate command to maintain the current longitudinal position. The longitudinal rate command is sent to the the longitudinal component of the Translational Rate Control outer-loop control system.

LonVel-RC/H For Longitudinal Velocity Rate Command / Longitudinal Velocity Hold, a constant inceptor deflection results in a constant commanded longitudinal velocity rate (i.e. forward ground relative acceleration). Releasing the inceptor back to a neutral position maintains the current commanded longitudinal velocity (i.e., forward ground relative velocity). The longitudinal velocity command is sent to the Acceleration Control outer-loop control system.

Spd-RC/H For Speed Rate Command / Speed Hold, constant inceptor deflection results in a constant commanded speed rate (i.e., acceleration). Releasing the inceptor back to the neutral position results in a zero speed rate command to maintain the current speed. The speed rate command is sent to the Acceleration Control outer-loop control system.

3. Target Rate Command Target Hold

In this category of command response, a constant inceptor deflection results in a constant rate of change in the commanded target. Releasing the inceptor back to the neutral position maintains the current commanded target. Fig. 20 shows the block diagram of the target rate command target hold function. Pilot inputs are scaled over the allowable range in the commanded rate of change. Subsequently, the target rate command is saturated by flight envelope limits and protected against windup. Next this commanded rate is integrated towards a commanded target state. This target state command is again constrained between saturation limits that are based on flight envelope limits. Next, this target command is fed through a first-order lag filter with a time constant that serves as a reference model. For the ultimate commanded target that is fed to the outer-loop controller, a feedforward term is added consisting of the saturated target rate command scaled by a time constant. This feedfoward signal removes much of the time delay in the vehicle response. A high-level description of the command response types that fit under this category are described below.

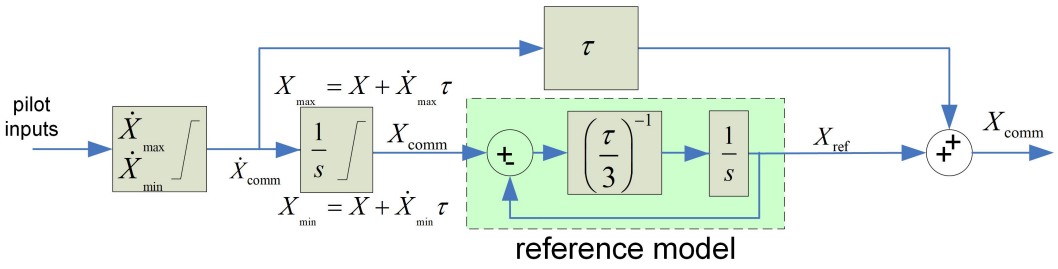

Fig. 20 Block diagram of the target rate command target hold function

AltTgt-RC/H For Altitude Target Rate Command / Altitude Target Hold, a constant inceptor deflection results in a constant rate of change in the commanded altitude target. Releasing the inceptor back to the neutral position maintains the current commanded altitude target. The commanded altitude target is sent to the Altitude Control outer-loop control system.

FpaTgt-RC/H For Flight Path Angle Target Rate Command / Flight Path Angle Target Hold, a constant inceptor deflection results in a constant rate of change in the commanded flight path angle target. Releasing the inceptor back to the neutral position maintains the current commanded flight path angle target. The commanded flight path angle target is sent to the Flight Path Angle Control outer-loop control system.

LatVelTgt-RC/Trk-H For Lateral Velocity Target Rate Command / Track Hold, a constant inceptor deflection results in a constant rate of change in the commanded lateral velocity target. Releasing the inceptor back to a neutral position maintains the current track angle. This is achieved by augmenting the commanded lateral velocity target with a correction term so that track angle remains steady during acceleration or deceleration. The underlying concept is as follows. The track angle χ is defined as follows:

$$\chi = \arctan \frac{V_{\text{gnd}_{\text{East}}}}{V_{\text{gnd}_{\text{North}}}} \tag{53}$$

where $V_{\text{gnd}_{\text{East}}}$ is the East component of the earth referenced ground velocity vector and $V_{\text{gnd}_{\text{North}}}$ is the North component. The time derivative of the track angle is then derived as follows by means of the chain rule:

$$\dot{\chi} = \frac{1}{1 + \left(\frac{V_{\text{gnd}_{\text{East}}}}{V_{\text{gnd}_{\text{North}}}}\right)^2} \frac{d}{dt}\left(\frac{V_{\text{gnd}_{\text{East}}}}{V_{\text{gnd}_{\text{North}}}}\right) = \frac{\dot{V}_{\text{gnd}_{\text{East}}} V_{\text{gnd}_{\text{North}}} - \dot{V}_{\text{gnd}_{\text{North}}} V_{\text{gnd}_{\text{East}}}}{V^2_{\text{gnd}_{\text{North}}} + V^2_{\text{gnd}_{\text{East}}}} \tag{54}$$

For a steady track angle, one needs $\dot{\chi} = 0$, which results in the requirement that $\dot{V}_{\text{gnd}_{\text{East}}} V_{\text{gnd}_{\text{North}}} - \dot{V}_{\text{gnd}_{\text{North}}} V_{\text{gnd}_{\text{East}}} = 0$ for a nonzero denominator. This results in the following correction term for the lateral acceleration (after rotating all velocity components over ψ from North-East reference frame to body fixed reference frame):

$$\dot{V}_{\text{gnd}_{\text{Y}}} = \frac{V_{\text{gnd}_{\text{Y}}}}{V_{\text{gnd}_{\text{X}}}} \dot{V}_{\text{gnd}_{\text{X}}} \tag{55}$$

Thus, an additional track angle acceleration or deceleration term is needed before the usual rate-to-angle integrator:

- forward groundspeed $V_{\text{gnd}_{\text{X}}} > 0$:

$$\Delta\dot{V}_{Y_{\text{cmd}}} = \frac{V_{Y_{\text{cmd}}} \cdot \dot{V}_{\text{gnd}_{\text{X}}}}{\underline{V_{\text{gnd}_{\text{X}}}}} \tag{56}$$

- backward groundspeed $V_{\text{gnd}_{\text{X}}} < 0$:

$$\Delta\dot{V}_{Y_{\text{cmd}}} = \frac{V_{Y_{\text{cmd}}} \cdot \dot{V}_{\text{gnd}_{\text{X}}}}{\overline{V_{\text{gnd}_{\text{X}}}}} \tag{57}$$

Please note that both $V_{\text{gnd}_{\text{X}}}$ and $\dot{V}_{\text{gnd}_{\text{X}}}$ are defined in the body fixed reference frame (along the nose of the vehicle). The singularity protected denominators in Eq. 56 and 57 are defined as follows:

$$\underline{V_{\text{gnd}_{\text{X}}}} = \max\left(V_{\text{gnd}_{\text{X}}}, 20kts\right) \tag{58}$$

$$\overline{V_{\text{gnd}_{\text{X}}}} = \min\left(V_{\text{gnd}_{\text{X}}}, -20kts\right) \tag{59}$$

The resulting commanded lateral velocity target is sent to the lateral component of the Translational Rate Control outer-loop control system.

LatPosTgt-RC/H and LonPosTgt-RC/H The Position Target Rate Command / Position Target Hold response is separated into a lateral component (i.e., Lateral Target Rate Command / Lateral Target Hold) and a longitudinal component (i.e., Longitudinal Target Rate Command / Longitudinal Target Hold). Constant inceptor deflections result in constant rates of change in the commanded target position along the respective (lateral and longitudinal) axes. Releasing the inceptors back to the neutral positions will maintain the current commanded target position. Pilot inputs are scaled over the command range between $+20kts$ and $-20kts$. Subsequently, the command is protected against windup. Next this commanded rate is integrated towards a commanded position and converted to lat/lon coordinates as follows:

$$\Delta\text{lat}_{\text{X}} = V_{X_{\text{cmd}}} dt \cdot \frac{\cos\psi}{R_e} \cdot \frac{180}{\pi} \tag{60}$$

$$\Delta\text{lon}_{\text{X}} = V_{X_{\text{cmd}}} dt \cdot \frac{\sin\psi}{R_e \cos\text{lat}} \cdot \frac{180}{\pi} \tag{61}$$

$$\Delta\text{lat}_{\text{Y}} = V_{Y_{\text{cmd}}} dt \cdot \frac{-\sin\psi}{R_e} \cdot \frac{180}{\pi} \tag{62}$$

$$\Delta\text{lon}_{\text{Y}} = V_{Y_{\text{cmd}}} dt \cdot \frac{\cos\psi}{R_e \cos\text{lat}} \cdot \frac{180}{\pi} \tag{63}$$

Next the position command distances are computed (with $\text{lat}_{\text{cmd}} = \sum \Delta\text{lat}_\text{X} + \sum \Delta\text{lat}_\text{Y}$ and $\text{lon}_{\text{cmd}} = \sum \Delta\text{lon}_\text{X} + \sum \Delta\text{lon}_\text{Y}$):

$$N = (\text{lat}_{\text{cmd}} - \text{lat}) \cdot \frac{\pi}{180} \cdot R_e \tag{64}$$

$$E = (\text{lon}_{\text{cmd}} - \text{lon}) \cdot \frac{\pi}{180} \cdot R_e \cos \text{lat} \tag{65}$$

$$X = N \cos\psi + E \sin\psi \tag{66}$$

$$Y = E \cos\psi - N \sin\psi \tag{67}$$

The next step is to limit the position command distances for X and Y in Eq. 66–67 between the limits $20kts \cdot \tau_{\text{pos}}$ and $-20kts \cdot \tau_{\text{pos}}$, where $\tau_{\text{pos}} = 3 \cdot \max\left(\tau_\phi, \tau_\theta\right)$. Finally the limited position command is computed with the reverse eq. 64 – 67. The speed control targets are calculated as follows:

$$V_{X_{\text{cmd}}} = \frac{1}{\tau_{\text{pos}}} X \tag{68}$$

$$V_{Y_{\text{cmd}}} = \frac{1}{\tau_{\text{pos}}} Y \tag{69}$$

The resulting commanded lateral and longitudinal velocities are sent to the Translational Rate Control outer loop control system.

SpdTgt-RC/H For Speed Target Rate Command / Speed Target Hold, a constant inceptor deflection results in a constant rate of change in the commanded speed target. Releasing the inceptor back to the neutral position maintains the current commanded speed target. The commanded speed target is sent to the Speed Control outer-loop control system. As the aircraft transitions through flight regimes, the speed target transitions over various reference speeds to ease operation. Airspeed applies in WBL and transitions to groundspeed in TBL. At the lowest speeds, the system commands only a forward groundspeed. As the vehicle picks up speed, this blends from a forward groundspeed, to groundspeed, to calibrated airspeed.

TrkTgt-RC/H For Track Target Rate Command / Track Target Hold, a constant inceptor deflection results in a constant rate of change in the commanded track angle target. Releasing the inceptor back to the neutral position maintains the current commanded track angle target. The maximum change in track angle command $\Delta\chi$ is limited based on the maximum turn rate as follows:

$$\chi_{\text{cmd}} = \chi + \Delta\chi_{\text{cmd}} \tag{70}$$

where the commanded change in track angle $\Delta\chi_{\text{cmd}}$ is restricted between the two limits:

$$\Delta\chi_{\text{max}} = \min\left(\dot{\psi}_{\text{max}} \cdot \tau_\chi, 45deg\right) \tag{71}$$

$$\Delta\chi_{\text{min}} = \max\left(\dot{\psi}_{\text{min}} \cdot \tau_\chi, -45deg\right) \tag{72}$$

The resulting commanded track angle target is sent to the Track Control outer-loop control system.

VspdTgt-RC/Fpa-H For Vertical Speed Target Rate Command / Flight Path Angle Hold, a constant inceptor deflection results in a constant rate of change in the commanded vertical speed target. Releasing the inceptor back to a neutral position maintains the current flight path angle. This is achieved by augmenting the commanded vertical velocity target with a correction term so that flight path angle remains steady during acceleration or deceleration. The underlying concept is as follows. The flight path angle γ is defined as follows:

$$\gamma = \arctan \frac{V_{\text{gnd}_\text{Z}}}{V_{\text{gnd}_\text{X}}} \tag{73}$$

where V_{gnd_Z} is the vertical component of the earth referenced velocity vector and V_{gnd_X} is the forward component along the flight path. The time derivative of the flight path angle is then derived as follows by means of the chain rule:

$$\dot{\gamma} = \frac{1}{1 + \left(\frac{V_{\text{gnd}_\text{Z}}}{V_{\text{gnd}_\text{X}}}\right)^2} \frac{d}{dt}\left(\frac{V_{\text{gnd}_\text{Z}}}{V_{\text{gnd}_\text{X}}}\right) = \frac{\dot{V}_{\text{gnd}_\text{Z}} V_{\text{gnd}_\text{X}} - \dot{V}_{\text{gnd}_\text{X}} V_{\text{gnd}_\text{Z}}}{V^2_{\text{gnd}_\text{X}} + V^2_{\text{gnd}_\text{Z}}} \tag{74}$$

For a steady flight path angle, one needs $\dot{\gamma} = 0$, which results in the requirement that $\dot{V}_{\text{gnd}_Z} V_{\text{gnd}_X} - \dot{V}_{\text{gnd}_X} V_{\text{gnd}_Z} = 0$ for a nonzero denominator. This results in the following correction term for the vertical acceleration:

$$\dot{V}_{\text{gnd}_Z} = \frac{V_{\text{gnd}_Z}}{V_{\text{gnd}_X}} \dot{V}_{\text{gnd}_X} \tag{75}$$

Thus, an additional flight path angle acceleration or deceleration term is needed before the usual rate-to-angle integrator, as follows:

- forward groundspeed $V_{\text{gnd}_X} > 0$:

$$\Delta\dot{V}_{Z_{\text{cmd}}} = \frac{V_{Z_{\text{cmd}}} \cdot \dot{V}_{\text{gnd}_X}}{\underline{V_{\text{gnd}_X}}} \tag{76}$$

- backward groundspeed $V_{\text{gnd}_X} < 0$:

$$\Delta\dot{V}_{Z_{\text{cmd}}} = \frac{V_{Z_{\text{cmd}}} \cdot \dot{V}_{\text{gnd}_X}}{\overline{V_{\text{gnd}_X}}} \tag{77}$$

Please note that both V_{gnd_X} and $\dot{V}_{\text{gnd}_X}$ are defined in the body fixed reference frame (along the nose of the vehicle). The singularity protected denominators in Eq. 76 and 77 are defined as follows:

$$\underline{V_{\text{gnd}_X}} = \max\left(V_{\text{gnd}_X}, 20kts\right) \tag{78}$$

$$\overline{V_{\text{gnd}_X}} = \min\left(V_{\text{gnd}_X}, -20kts\right) \tag{79}$$

This singularity protection also makes the commanded flight path level off when approaching hover. Moreover, the vertical acceleration limits are defined as follows: $\dot{V}_{Z_{\max}} = \frac{V_{Z_{\max}}}{\tau_\gamma}$ and $\dot{V}_{Z_{\min}} = \frac{V_{Z_{\min}}}{\tau_\gamma}$. The resulting commanded vertical speed target is sent to the Vertical Speed Control outer-loop control system.

D. Outer Loop Control Systems

There are 16 different outer loop control systems introduced in Fig. 13, which are all explained below. They are broken down by category:

- Euler and aerodynamic angles and rates
- Navigation angles and rates
- Altitude and vertical speed
- Speed and acceleration

1. Euler and aerodynamic angles and rates

Bank Control For bank angle control, the commanded bank angle ϕ_{cmd} is limited between the maximum authority limits $\phi_{\min}$ and $\phi_{\max}$, and maximum envelope limits if applicable. Next, ϕ_{cmd} is used to calculate the controlled earth referenced roll rate $\dot{\phi}_{\text{cmd}}$, based on the roll time constant τ_ϕ, as follows:

$$\dot{\phi}_{\text{cmd}} = \frac{1}{\tau_\phi}\left(\phi_{\text{cmd}} - \phi\right) \tag{80}$$

This roll rate is subsequently fed to the bank rate control module, before being passed to the RCAH inner loop.

Bank Rate Control For bank rate control, the commanded bank rate, either earth referenced $\dot{\phi}_{\text{cmd}}$ or body fixed p_{cmd} is limited between their respective maximum authority limits $\dot{\phi}_{\min}$ and $\dot{\phi}_{\max}$ or $p_{\min}$ and $p_{\max}$, and maximum envelope limits if applicable.

Subsequently, a coordinate transformation is performed, depending on the direction of the change in reference frame:

- From body fixed to earth referenced:

$$\dot{\phi}_{\text{cmd}} = p_{\text{cmd}} + \dot{\psi}\sin\theta \tag{81}$$

- From earth referenced to body fixed:

$$p_{\text{cmd}} = \dot{\phi}_{\text{cmd}} - \dot{\psi}\sin\theta \tag{82}$$

This bank rate is subsequently passed to the RCAH inner loop.

Heading Control For heading control, the commanded heading ψ_{cmd} is used to calculate the controlled earth referenced heading rate $\dot{\psi}_{\text{cmd}}$, based on the heading time constant τ_{ψ}, as follows:

$$\dot{\psi}_{\text{cmd}} = \frac{1}{\tau_{\psi}} \left(\psi_{\text{cmd}} - \psi\right) \tag{83}$$

Heading Rate Control Commanded earth referenced yaw rate $\dot{\psi}_{\text{cmd}}$ is limited between its extreme authority limits.

If a non-zero sideslip angle is commanded (in turn coordination): Compensate for commanded change in sideslip angle:

$$\dot{\psi}_{\text{cmd}_{\text{corr}_1}} = \dot{\psi}_{\text{cmd}} + \dot{\beta}_{\text{cmd}} \tag{84}$$

where:

$$\dot{\beta}_{\text{cmd}} = \frac{1}{\tau_{\beta}} \left(\beta_{\text{cmd}} - \beta\right) \tag{85}$$

The commanded earth referenced yaw rate $\dot{\psi}_{\text{cmd}}$ is limited between its envelope limits. Heading rate is either controlled directly via the RCDH inner loop control mode when it is active, otherwise heading rate control is achieved via bank. First compensate for increased heading rate due to level-turn compensation:

$$\dot{\psi}_{\text{cmd}_{\text{corr}_2}} = \dot{\psi}_{\text{cmd}_{\text{corr}_1}} \cos\theta \tag{86}$$

Subsequently, the commanded bank angle is calculated and limited between authority limits and, if applicable, envelope limits:

$$\phi_{\text{cmd}} = \arctan \dot{\psi}_{\text{cmd}} \frac{V_{\text{TAS}}}{g} \tag{87}$$

This value is then fed to the aforementioned bank control law.

Pitch Angle Control For pitch angle control, the commanded pitch attitude angle θ_{cmd} is limited between the maximum authority limits θ_{min} and θ_{max}, and maximum envelope limits if applicable. Next, θ_{cmd} is used to calculate the controlled earth referenced pitch rate $\dot{\theta}_{\text{cmd}}$, based on the pitch time constant τ_{θ}, as follows:

$$\dot{\theta}_{\text{cmd}} = \frac{1}{\tau_{\theta}} \left(\theta_{\text{cmd}} - \theta\right) \tag{88}$$

This pitch rate is subsequently fed to the pitch rate control module, before being passed to the RCAH inner loop.

Pitch Rate Control For pitch rate control, the commanded pitch rate, either earth referenced $\dot{\theta}_{\text{cmd}}$ or body fixed q_{cmd} is limited between their respective maximum authority limits $\dot{\theta}_{\text{min}}$ and $\dot{\theta}_{\text{max}}$ or q_{min} and q_{max}, and maximum envelope limits if applicable.

Subsequently, a coordinate transformation is performed, depending on the direction of the change in reference frame:

- From body fixed to earth referenced:

$$\dot{\theta}_{\text{cmd}} = \left(q_{\text{cmd}} - \dot{\psi}\cos\theta\sin\phi\right) \frac{1}{\cos\phi} \tag{89}$$

- From earth referenced to body fixed:

$$q_{\text{cmd}} = \dot{\theta}_{\text{cmd}}\cos\phi + \dot{\psi}\cos\theta\sin\phi \tag{90}$$

This pitch rate is subsequently passed to the RCAH inner loop.

Sideslip Control For sideslip control, the commanded sideslip angle β_{cmd} is limited between the maximum authority limits β_{min} and β_{max}, and subsequently fed to the turn coordination (TC) inner loop control module.

2. Navigation angles and rates

Flight Path Angle Control For flight path angle control, the commanded flight path angle γ_{cmd} is limited between the maximum authority limits γ_{min} and γ_{max} and maximum envelope limits if applicable, and subsequently used to control the flight path angle either by heave via $\dot{h}_{\text{cmd}}$ or by pitch via $\dot{\gamma}_{\text{cmd}}$.
For flight path angle by heave:

$$\dot{h}_{\text{cmd}} = \tan \gamma_{\text{cmd}} \cdot V_{\text{gnd}_{\text{lim}}} \tag{91}$$

where $V_{\text{gnd}_{\text{lim}}}$ is the lower value limited ground speed, defined as follows:

$$V_{\text{gnd}_{\text{lim}}} = \max \left(V_{\text{gnd}}, 20kts \right) \tag{92}$$

The commanded vertical speed $\dot{h}_{\text{cmd}}$ is then limited between the maximum authority limits $\dot{h}_{\text{min}}$ and $\dot{h}_{\text{max}}$ and maximum envelope limits if applicable. Either via Flight Path Angle Rate Control or otherwise directly, $\dot{h}_{\text{cmd}}$ is fed to the vertical speed control module which connects it to the inner loop RCHH control.
For flight path angle by pitch:

$$\dot{\gamma}_{\text{cmd}} = \frac{1}{\tau_\gamma} \left(\gamma_{\text{cmd}} - \gamma \right) \tag{93}$$

This $\dot{\gamma}_{\text{cmd}}$ value is then used as commanded value for flight path angle rate control.

Flight Path Angle Rate Control For flight path angle rate control, the commanded flight path angle rate $\dot{\gamma}_{\text{cmd}}$ is limited between the maximum envelope limits $\dot{\gamma}_{\text{min}_{\text{env}}}$ and $\dot{\gamma}_{\text{max}_{\text{env}}}$ if applicable, and subsequently used to control the flight path angle rate either by heave via $\dot{h}_{\text{cmd}}$ or by pitch via θ_{cmd}.
For flight path angle rate by heave:
First the commanded flight path angle is calculated:

$$\gamma_{\text{cmd}} = \gamma + \tau_\gamma \dot{\gamma}_{\text{cmd}} \tag{94}$$

This commanded flight path angle γ_{cmd} is then limited between the maximum authority limits γ_{min} and γ_{max} and maximum envelope limits if applicable, and subsequently used to calculate the commanded vertical speed:

$$\dot{h}_{\text{cmd}} = \tan \gamma_{\text{cmd}} \cdot V_{\text{gnd}} \tag{95}$$

where V_{gnd} is the ground speed. Next, $\dot{h}_{\text{cmd}}$ is fed to the inner loop RCHH control.
For flight path angle rate by pitch:
Assuming that the commanded pitch rate can be approximated by the commanded flight path angle rate: $\dot{\theta}_{\text{cmd}} = \dot{\gamma}_{\text{cmd}}$, the commanded pitch attitude angle θ_{cmd} is calculated as follows:

$$\theta_{\text{cmd}} = \theta + \tau_\theta \dot{\theta}_{\text{cmd}} \tag{96}$$

This commanded pitch attitude angle θ_{cmd} is then used as command value for the pitch control module in ACAH mode, or $\dot{\theta}_{\text{cmd}} = \dot{\gamma}_{\text{cmd}}$ is used as command value for the pitch rate control module in RCAH mode.

At low speeds, since angles may be ill-defined and sensitive, commands are formulated as axial speed component commands (vertical speed). The use of a synthetic flight path angle ensures a smooth transition from a true flight path angle command to essentially a vertical speed command. The crossover between true and synthetic angle takes place at the speed where a flight path angle of 1 deg corresponds to a vertical speed component of 1 ft/s, which is around $V_{\text{gnd}} = 34$ kts.

Track Control For track control, the commanded track angle χ_{cmd} is used to calculate the commanded track rate $\dot{\chi}_{\text{cmd}}$, based on the track time constant τ_χ, as follows:

$$\dot{\chi}_{\text{cmd}} = \frac{1}{\tau_\chi} \left(\chi_{\text{cmd}} - \chi \right) \tag{97}$$

This commanded track rate $\dot{\chi}_{\text{cmd}}$ is then fed to the track rate control module.

Track Rate Control Commanded track rate $\dot{\chi}_{\text{cmd}}$ is limited between the maximum authority limits $\dot{\psi}_{\text{min}}$ and $\dot{\psi}_{\text{max}}$ and maximum envelope limits $\dot{\psi}_{\text{min}_{\text{env}}}$ and $\dot{\psi}_{\text{max}_{\text{env}}}$ if applicable, and subsequently used to control the track rate by bank. "Track by bank" is achieved either directly via ϕ_{cmd} or indirectly via the lateral ground speed $v_{\text{gnd}_{\text{cmd}}}$.
Track rate control by yaw (when TRC is active):
Assuming that the commanded yaw rate can be approximated by the commanded track rate: $\dot{\psi}_{\text{cmd}} = \dot{\chi}_{\text{cmd}}$
Track rate control by bank:
In this specific non-conventional flight condition, one needs to calculate the commanded bank angle for controlling track rate but in the presence of significant sideslip. The derivation follows next. The applicable Free Body Diagram of the governing forces is shown in Fig. 21.

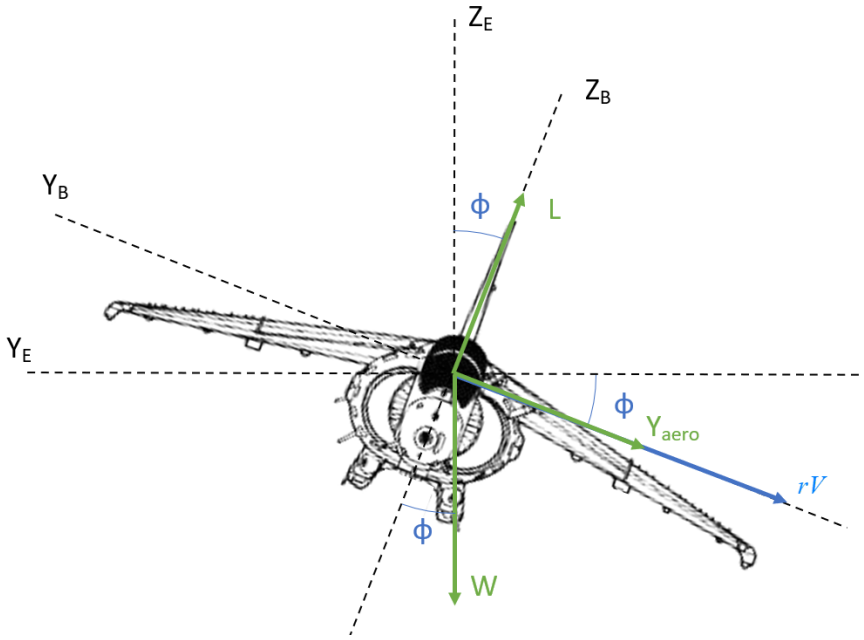

Fig. 21 Governing forces in turning flight along the Y_B and Z_B axes

The equation of motion along the body Y-axis Y_B is as follows:

$$W \sin\phi + Y_{\text{aero}} = mVr \tag{98}$$

where Y_{aero} is the aerodynamic sideforce, which is caused by the sideslipping flight. The inverse Euler equation for the body axis yaw rate r is defined as:

$$r = \dot{\psi}\cos\phi\cos\theta - \dot{\theta}\sin\phi \tag{99}$$

Combining Eq. 98 and 99 results in:

$$W \sin\phi + Y_{\text{aero}} = mV\left(\dot{\psi}\cos\phi\cos\theta - \dot{\theta}\sin\phi\right) \tag{100}$$

Next substituting $W = mg$ and $Y_{\text{aero}} = n_Y W = n_Y mg$:

$$mg \sin\phi + n_Y mg = mV\left(\dot{\psi}\cos\phi\cos\theta - \dot{\theta}\sin\phi\right) \tag{101}$$

Eliminating the common mass factor m and regrouping for the ϕ terms:

$$\left(g + V\dot{\theta}\right)\sin\phi - \left(V\cos\theta\dot{\psi}\right)\cos\phi = -gn_Y \tag{102}$$

Solving for bank angle ϕ results in the equation, where the relevant required variables are used where necessary:

$$\phi_{\text{cmd}} = \arccos\left(\frac{-gn_Y}{\sqrt{\left(g + V\dot{\theta}_{\text{cmd}}\right)^2 + \left(V\cos\theta\dot{\psi}_{\text{cmd}}\right)^2}}\right) + \arctan\left(-\frac{g + V\dot{\theta}_{\text{cmd}}}{V\cos\theta\dot{\psi}_{\text{cmd}}}\right) \tag{103}$$

where the commanded track rate is adjusted for level turns: $\dot{\psi}_{\text{cmd}} = \dot{\chi}_{\text{cmd}} \cos\theta$.

This result is achieved by using the universal relationship:

$$a \sin\phi - b \cos\phi = c \quad \Longleftrightarrow \quad \phi = \arccos\left(\frac{c}{\sqrt{a^2+b^2}}\right) + \arctan\left(-\frac{a}{b}\right) \tag{104}$$

Eq. 103 was validated for specific situations of straight sideslipping flight, where it simplifies to $\phi_{\text{cmd}} = \arcsin(-n_Y)$ and for level turn coordinated (zero sideslip) flight, where it simplifies to $\phi_{\text{cmd}} = \arctan\left(\dot{\psi}_{\text{cmd}} \frac{V}{g}\right)$. The commanded bank angle value ϕ_{cmd} from Eq. 103 is then fed to the bank control module.

At low speeds, since angles may be ill-defined and sensitive, commands are formulated as axial speed component commands (lateral speed). The use of a synthetic track angle ensures a smooth transition from a true track angle command to essentially a lateral ground speed command. The crossover between true and synthetic angle takes place at the speed where a track angle of 1 deg corresponds to a lateral ground speed component of 1 ft/s, which is around $V_{\text{gnd}} = 34$ kts.

Translational Rate Control (TRC) Translational Rate Command is a dedicated mode which is used in the landing phase and for precision maneuvering with respect to the ground. Longitudinal and lateral stick deflections command the forward and sideways inertial speed components respectively. The derivation of how these inertial speed components map to the pitch and roll angles is shown below.

This kinematic relationship shows how the translational rate components are related to the Euler angles[25]:

$$\begin{bmatrix} \ddot{x}_{\text{gnd}} \\ \ddot{y}_{\text{gnd}} \\ \ddot{z}_{\text{gnd}} \end{bmatrix} = \begin{bmatrix} 0 \\ 0 \\ g \end{bmatrix} + \frac{1}{m} \mathbf{\Omega}_{\psi}^{-1} \mathbf{\Omega}_{\theta}^{-1} \mathbf{\Omega}_{\phi}^{-1} \left(\begin{bmatrix} \bar{q} S C_{X_B} \\ \bar{q} S C_{Y_B} \\ \bar{q} S C_{Z_B} \end{bmatrix} + \begin{bmatrix} T \cos\delta_T \\ 0 \\ T \sin\delta_T \end{bmatrix} \right) \tag{105}$$

where the body force components are defined by the aerodynamic forces as follows:

$$\begin{bmatrix} \bar{q} S C_{X_B} \\ \bar{q} S C_{Y_B} \\ \bar{q} S C_{Z_B} \end{bmatrix} = \bar{q} S \mathbf{\Omega}_{\alpha}^{-1} \mathbf{\Omega}_{\beta}^{-1} \begin{bmatrix} -C_{D_{\text{aero}}} \\ C_{Y_{\text{aero}}} \\ -C_{L_{\text{aero}}} \end{bmatrix} \tag{106}$$

Simplifying by assuming that only the vertical rotors are used in the hover phase and that the aerodynamic influences are negligible due to the low airspeed, results in:

$$m \mathbf{\Omega}_{\psi} \begin{bmatrix} \ddot{x}_{\text{gnd}} \\ \ddot{y}_{\text{gnd}} \\ \ddot{z}_{\text{gnd}} - g \end{bmatrix} = \mathbf{\Omega}_{\theta}^{-1} \mathbf{\Omega}_{\phi}^{-1} \begin{bmatrix} 0 \\ 0 \\ T \sin\delta_T \end{bmatrix} \tag{107}$$

Expanding these matrix equations results in:

$$\begin{bmatrix} m\left(\ddot{x}_{\text{gnd}} \cos\psi + \ddot{y}_{\text{gnd}} \sin\psi\right) \\ m\left(\ddot{y}_{\text{gnd}} \cos\psi - \ddot{x}_{\text{gnd}} \sin\psi\right) \\ m\left(\ddot{z}_{\text{gnd}} - g\right) \end{bmatrix} = \begin{bmatrix} \cos\phi \sin\theta T \sin\delta_T \\ -\sin\phi T \sin\delta_T \\ \cos\phi \cos\theta T \sin\delta_T \end{bmatrix} \tag{108}$$

Solving for pitch angle θ and bank angle ϕ results in:

$$\tan\theta = \frac{\ddot{x}_{\text{gnd}} \cos\psi + \ddot{y}_{\text{gnd}} \sin\psi}{\ddot{z}_{\text{gnd}} - g} \tag{109}$$

$$\sin\phi = -\frac{m\left(\ddot{y}_{\text{gnd}} \cos\psi - \ddot{x}_{\text{gnd}} \sin\psi\right)}{T \sin\delta_T} \tag{110}$$

Besides it can be found that:

$$m \left\| \begin{matrix} \ddot{x}_{\text{gnd}} \\ \ddot{y}_{\text{gnd}} \\ \ddot{z}_{\text{gnd}} - g \end{matrix} \right\|_2 = \left\| \begin{matrix} 0 \\ 0 \\ T \sin\delta_T \end{matrix} \right\|_2 \tag{111}$$

And thus:

$$T \sin \delta_T = m\sqrt{\ddot{x}_{\text{gnd}}^2 + \ddot{y}_{\text{gnd}}^2 + \left(\ddot{z}_{\text{gnd}} - g\right)^2} \tag{112}$$

Implementing Eq. (112) in Eq. (110) results in the following equations for required pitch attitude and bank angles based on the required translational accelerations, and which are independent of any airframe information:

$$\theta_{\text{req}} = \arctan \frac{\ddot{x}_{\text{gnd}_{\text{req}}} \cos\psi + \ddot{y}_{\text{gnd}_{\text{req}}} \sin\psi}{\ddot{z}_{\text{gnd}_{\text{req}}} - g} \tag{113}$$

$$\phi_{\text{req}} = -\arcsin \frac{\left(\ddot{y}_{\text{gnd}_{\text{req}}} \cos\psi - \ddot{x}_{\text{gnd}_{\text{req}}} \sin\psi\right)}{\sqrt{\ddot{x}_{\text{gnd}_{\text{req}}}^2 + \ddot{y}_{\text{gnd}_{\text{req}}}^2 + \left(\ddot{z}_{\text{gnd}_{\text{req}}} - g\right)^2}} \tag{114}$$

Because of the relative degree, the linear controllers of the two TRC channels work up to the second order derivative, and they have the following control law:

$$\nu_{\ddot{x}} = \ddot{x}_{\text{gnd}_{\text{req}}} = \left(K_{\dot{x}} + \frac{K_{\dot{x}_I}}{s}\right)\left(\dot{x}_{\text{gnd}_{\text{ref}}} - \dot{x}_{\text{gnd}}\right) + K_{\ddot{x}}\left(\ddot{x}_{\text{gnd}_{\text{ref}}}\right) \tag{115}$$

$$\nu_{\ddot{y}} = \ddot{y}_{\text{gnd}_{\text{req}}} = \left(K_{\dot{y}} + \frac{K_{\dot{y}_I}}{s}\right)\left(\dot{y}_{\text{gnd}_{\text{ref}}} - \dot{y}_{\text{gnd}}\right) + K_{\ddot{y}}\left(\ddot{y}_{\text{gnd}_{\text{ref}}}\right) \tag{116}$$

$$\nu_{\ddot{z}} = \ddot{z}_{\text{gnd}_{\text{req}}} = K_{\dot{z}}\left(\dot{z}_{\text{gnd}_{\text{req}}} - \dot{z}_{\text{gnd}}\right) \tag{117}$$

The values of the controller gains mentioned in Eq. (115)–(117) are specified in Table 1. The second order time derivatives of the control commands used in Eq. (115)–(117) are fed forward internal signals from the first order reference models for the two TRC channels:

$$H_{\text{ref}}(s) = \frac{1}{T_V s + 1} \tag{118}$$

The value for the time constant in Eq. (118) is $T_V = 3s$ and was chosen such that the reference model satisfies the ADS-33 Flying and Handling Quality requirements. Fig. 22 shows the interconnections between reference model, linear controller and kinematics inversion for TRC.

Table 1 Linear controller gains for Eq. (115)–(117)

axis	rate	acceleration
longitudinal & lateral	$K_{\dot{x}/\dot{y}/\dot{z}} = 2 * 0.25$ $K_{\dot{x}/\dot{y}_I} = 0.25^2$	$K_{\ddot{x}/\ddot{y}} = 1$
yaw	$K_{\psi} = 6$	$K_{\dot{\psi}} = 5$

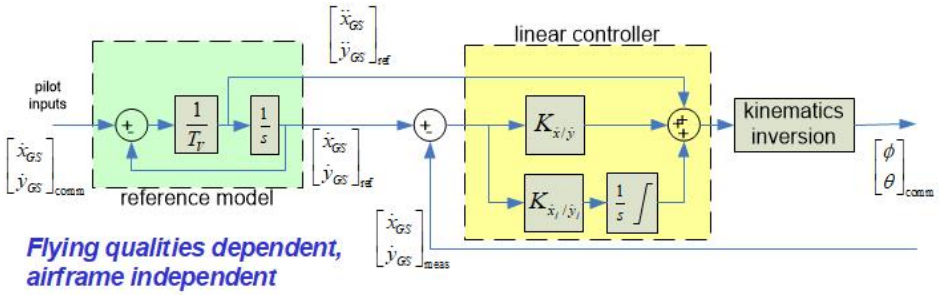

Fig. 22 Detailed overview of the control structure and interconnections for TRC (translational rate control)

3. Altitude and vertical speed

Altitude Control For altitude control, the commanded altitude h_{cmd} is used to calculate the controlled earth referenced vertical speed $\dot{h}_{\text{cmd}}$, based on the altitude time constant τ_h, as follows:

$$\dot{h}_{\text{cmd}} = \frac{1}{\tau_h}\left(h_{\text{cmd}} - h\right) \tag{119}$$

The vertical speed is then fed to vertical speed control.

Vertical Speed Control For vertical speed control, the commanded vertical speed $\dot{h}_{\text{cmd}}$ is limited between the maximum authority limits $\dot{h}_{\text{min}}$ and $\dot{h}_{\text{max}}$ and maximum envelope limits if applicable, and subsequently used to control the vertical speed either by heave via the RCHH inner loop control module or by pitch (rate) via $\theta_{\text{cmd}}/\dot{\theta}_{\text{cmd}}$.
Vertical speed by pitch (rate):
The commanded flight path angle γ_{cmd} is calculated as follows:

$$\gamma_{\text{cmd}} = \arctan\frac{\dot{h}_{\text{cmd}}}{V_{\text{gnd}_{\text{lim}}}} \tag{120}$$

where $V_{\text{gnd}_{\text{lim}}}$ is the singularity protected ground speed:

$$V_{\text{gnd}_{\text{lim}}} = \max\left(V_{\text{gnd}}, 10kts\right) \tag{121}$$

Next the commanded flight path rate $\dot{\gamma}_{\text{cmd}}$ is calculated, based on the flight path angle time constant τ_γ, as follows:

$$\dot{\gamma}_{\text{cmd}} = \frac{1}{\tau_\gamma}\left(\gamma_{\text{cmd}} - \gamma\right) \tag{122}$$

Both flight path angle and rate are limited between their maximum authority limits if the safe envelope is active. Assuming that the commanded pitch rate can be approximated by the commanded flight path angle rate: $\dot{\theta}_{\text{cmd}} = \dot{\gamma}_{\text{cmd}}$, the commanded pitch attitude angle θ_{cmd} is calculated as follows:

$$\theta_{\text{cmd}} = \theta + \tau_\theta \dot{\theta}_{\text{cmd}} \tag{123}$$

This commanded pitch attitude angle θ_{cmd} is then used as command value for the pitch control module in ACAH mode, or $\dot{\theta}_{\text{cmd}} = \dot{\gamma}_{\text{cmd}}$ is used as command value for the pitch rate control module in RCAH mode.

4. Speed and acceleration

Acceleration Control For acceleration control, the commanded acceleration $\dot{V}_{\text{cmd}}$ is limited between the maximum authority limits $\dot{V}_{\text{CAS}_{\text{min}}}$ and $\dot{V}_{\text{CAS}_{\text{max}}}$ and maximum envelope limits if applicable, and subsequently either passed directly to the ACSH inner loop control or otherwise used to calculate the commanded forward groundspeed for TRC.
For TRC:

$$\dot{x}_{\text{gnd}_{\text{cmd}}} = \dot{x}_{\text{gnd}} + \dot{V}_{\text{cmd}}\tau_V \tag{124}$$

Speed Control Speed is controlled either by pitch, using TRC, or by acceleration, using inner loop control ACSH, depending on the flight mode. For speed by pitch, the commanded speed V_{cmd} is used as the external TRC input for the commanded forward ground speed $\dot{x}_{\text{gnd}_{\text{cmd}}}$:

$$\dot{x}_{\text{gnd}_{\text{cmd}}} = V_{\text{cmd}} \tag{125}$$

For speed by acceleration, the commanded acceleration $\dot{V}_{\text{cmd}}$ is calculated as follows:

$$\dot{V}_{\text{cmd}} = \frac{1}{\tau_V}\Delta V \tag{126}$$

where the speed error ΔV is calculated as follows:

$$\Delta V = \left(V_{\text{cmd}} - V_{\text{CAS}_{\text{comp}}}\right) \tag{127}$$

where $V_{\text{CAS}_{\text{comp}}}$ is the computed calibrated airspeed. Outside hover the computed calibrated airspeed equals the calibrated airspeed V_{CAS}. In hover, the computed calibrated airspeed uses ground speed. ΔV is also limited between $\Delta V_{\text{max}} = V + \dot{V}_{\text{CAS}_{\text{max}}}\tau_V$ and $\Delta V_{\text{min}} = V + \dot{V}_{\text{CAS}_{\text{min}}}\tau_V$.

References

[1] VFS, "eVTOL Aircraft Directory," Online, 2022. URL https://evtol.news/aircraft/, retrieved March 20, 2022.

[2] Malpica, C., and Withrow-Maser, S., "Handling Qualities Investigation of Variable Blade Pitch and Variable Rotor Speed Controller eVTOL Quadrotor Concepts for Urban Air Mobility," *Proceedings of the VFS International Powered Lift Conference*, Vertical Flight Society, 2020.

[3] "A Rational Construct for Simplified Vehicle Operations (SVO)," Gama epic svo subcommittee whitepaper, Washington D.C. and Brussels, Belgium, May 2019. URL https://gama.aero/documents/svo-whitepaper-a-rationale-construct-for-simplified-vehicle-operations-svo-version-1-0-may2019/.

[4] Nicholas, O. P., and Bennett, P. J., "Proposed Wide Envelope Unified Control Concept for Vectored Thrust VSTOL Aircraft," Technical Memorandum FS312, Royal Aircraft Establishment RAE, Mar. 1980.

[5] Scott, R., *Aeroplane Monthly*, Key Publishing, 2020, Vol. 48, Chaps. VAAC HARRIER: How the oldest two-seat Harrier helped perfect the control method for today's F-35 Lightning II, pp. 92 – 99.

[6] Denham, J., "STOVL Integrated Flight and Propulsion Control: Current Successes and Remaining Challenges," *2002 Biennial International Powered Lift Conference and Exhibit*, American Institute of Aeronautics and Astronautics, 2002. doi:10.2514/6.2002-6021.

[7] Denham, J., and Paines, J., "Converging on a Precision Hover Control Strategy for the F-35B STOVL Aircraft," *AIAA Guidance, Navigation and Control Conference and Exhibit*, American Institute of Aeronautics and Astronautics, 2008. doi:10.2514/6.2008-6331.

[8] Stewart, E., "A piloted simulation study of advanced controls and displays for novice general aviation pilots," *32nd Aerospace Sciences Meeting and Exhibit*, American Institute of Aeronautics and Astronautics, 1994. doi:10.2514/6.1994-276.

[9] Kaneshige, J., Lombaerts, T., Shish, K., and Feary, M., "Command and Control Concepts for a Lift Plus Cruise Electric Vertical Takeoff and Landing Vehicle," *AIAA AVIATION 2023 FORUM*, American Institute of Aeronautics and Astronautics, 2023. doi:10.2514/6.2023-3910.

[10] Feary, M., Kaneshige, J., Haworth, L., Lombaerts, T., Shish, K., Iwai, N., and Archdeacon, J., "Evaluation of Novel V/STOL Aircraft Control for Expected AAM Operations," *AIAA AVIATION 2023 FORUM*, American Institute of Aeronautics and Astronautics, 2023. doi:10.2514/6.2023-3909.

[11] Lombaerts, T., Kaneshige, J., and Feary, M., "Control Concepts for Simplified Vehicle Operations of a Quadrotor eVTOL Vehicle," *AIAA AVIATION 2020 FORUM*, American Institute of Aeronautics and Astronautics, 2020. doi:10.2514/6.2020-3189.

[12] Silva, C., Johnson, W. R., Solis, E., Patterson, M. D., and Antcliff, K. R., "VTOL Urban Air Mobility Concept Vehicles for Technology Development," *2018 Aviation Technology, Integration, and Operations Conference*, American Institute of Aeronautics and Astronautics, 2018. doi:10.2514/6.2018-3847.

[13] Val, R. D., and He, C., "FLIGHTLAB^{TM} Modeling for Real Time Simulation Applications," *International Journal of Modeling Simulation and Scientific Computing*, Vol. 08, No. 4, 2017. doi:10.1142/S1793962317430036.

[14] Val, R. D., and He, C., "Validation of the FLIGHTLAB virtual engineering toolset," *The Aeronautical Journal*, Vol. 122, No. 1250, 2018, pp. 519–555. doi:10.1017/aer.2018.12.

[15] Zivan, L., and Tischler, M. B., "Development of a full flight envelope helicopter simulation using system identification," *Journal of the American Helicopter Society*, Vol. 55, No. 2, 2010. doi:10.4050/JAHS.55.022003.

[16] Tobias, E. L., Sanders, F. C., and Tischler, M. B., "Full-envelope stitched simulation model of a quadcopter using STITCH," *AHS International 74th Annual Forum & Technology Display*, Vertical Flight Society, 2018.

[17] "Realistic Gusting Crosswind Profiles for Flight Simulation Training Device (FSTD) Qualification," Tech. Rep. NSP GB 16-02, Federal Aviation Administration (FAA), May 2019. URL https://www.faa.gov/sites/faa.gov/files/about/initiatives/nsp/fstd_dir/16-02.pdf.

[18] Lombaerts, T., Kaneshige, J., Schuet, S., Hardy, G., Aponso, B. L., and Shish, K. H., "Nonlinear Dynamic Inversion Based Attitude Control for a hovering quad tiltrotor eVTOL vehicle," *AIAA Scitech 2019 Forum*, American Institute of Aeronautics and Astronautics, 2020. doi:10.2514/6.2019-0134.

[19] Lombaerts, T., Kaneshige, J., Schuet, S., Aponso, B. L., Shish, K. H., and Hardy, G., "Dynamic Inversion based Full Envelope Flight Control for an eVTOL Vehicle using a Unified Framework," *AIAA Scitech 2020 Forum*, American Institute of Aeronautics and Astronautics, 2020. doi:10.2514/6.2020-1619.

[20] "Aeronautical Design Standard, Performance Specification, Handling Qualities Requirements for Military Rotorcraft," Tech. Rep. ADS-33E-PRF, United States Army Aviation and Missile Command Aviation Engineering Directorate, Mar. 2000. URL https://www.amrdec.army.mil/amrdec/rdmr-se/tdmd/Documents/ads33front.pdf.

[21] Archdeacon, J. L., and Iwai, N., "Aerospace Cognitive Engineering Laboratory (ACELAB) Simulator for Urban Air Mobility (UAM) Research and Development," *AIAA AVIATION 2020 FORUM*, American Institute of Aeronautics and Astronautics, 2020. doi:10.2514/6.2020-3187.

[22] Decker, W. A., "Handling Qualities Evaluation of XV-15 Noise Abatement Landing Approaches Using a Flight Simulator," *American Helicopter Society 57th Annual Forum*, Washington D.C., 2001. URL https://rotorcraft.arc.nasa.gov/Publications/files/Decker.1CTR-8AHSPaper[1].pdf.

[23] Webber, D., "UAM Helicopter Surrogate Flight Test Report," techreport AAM-NC-070-001, NASA, 2022. URL https://www.faa.gov/training_testing/testing/test_standards/.

[24] Zahn, D., "personal communication," , 2022.

[25] Simplicio, P., Pavel, M., van Kampen, E., and Chu, Q., "An acceleration measurements-based approach for helicopter nonlinear flight control using Incremental Nonlinear Dynamic Inversion," *Control Engineering Practice*, Vol. 21, 2013, pp. 1065–1077. doi:10.1016/j.conengprac.2013.03.0009.